GRK 1782

"Functionalization of Semiconductors"

Seminar 2019

Haus Schönblick, Schwäbisch Gmünd, 23.09.2019 – 25.09.2019

Research Summaries

supported by: DFG Deutsche Forschungsgemeinschaft

Graduiertenkolleg 1782

„Functionalization of Semiconductors“

Haus Schönblick, Schwäbisch Gmünd

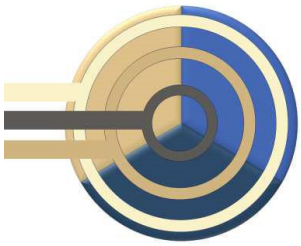

Seminar Program 23. – 25.09.2019

Monday, 23.09.2019

till 12:30	Arrival
13:00 – 14:00	Lunch
	Session I Chair: *Mikko Wilhelm*
14:00 – 14:30	***Alexa Adamkiewicz**:* Controlled Manipulation of Diethyl Ether on Si(001) via Tip-Induced Electronic Excitation
14:30 – 15:00	***Badal Mondal**:* Morphological stability analysis of (pseudo-) ternary epitaxial surface
15:00 – 15:30	***Fabian Pieck***: Automated exploration of reaction networks in chemical vapor deposition by density functional theory
15:30– 16:00	Coffee Break
	Session II Chair: *Oliver Maßmeyer*
16:00 – 16:30	***Luise Rost**:* Optical Spectroscopy of Ga(NAs)/Si and (GaIn)As/GaAs/Ga(AsSb) heterostructures
16:30 – 17:00	***Mikko Wilhelm**:* Optoelectronic coupling of colloidal quantum dots and semiconductor substrates
17:00 – 17:30	***Steven Youngkin**:* Investigation of coherent interface phonons in GaP/Si heterostructures by means of pump-probe differential reflection
18:00	Dinner

Tuesday, 24.09.2019

08:00 – 09:00 Breakfast

Session III Chair: *Marcel Köster*

09:00 – 09:30 ***Eike Dornsiepen****:* Organotetrelchalcogenide Clusters with Nonlinear Optical Properties
09:30 – 10:00 ***Thilo Hepp****:* MOVPE Growth of Ga(N,As)/Ga(As,Bi)/Ga(N,As) W Type Structures
10:00 – 10:30 ***Johannes Glowatzki****:* Nitrogen incorporation in GaP on Si/GaP using novel metal organic N P precursor di-tert-butyl-amino-phosphan (DTBAP)

10:30 – 11:00 Coffee Break

Session IV Chair: *Eike Dornsiepen*

11:00 – 11:30 ***Marcel Kröner****:* Optimization of Ga(N,As,Sb)/(B,Ga)(As,P)-heterostructures for laser applications on Si (001) substrate
11:30 – 12:00 ***Oliver Maßmeyer****:* Decomposition Analysis of TBAs and TBP during GaAs and GaP Growth by MOVPE
12:00 – 12:30 ***Christian Ritter****:* Building Interpnictogen Chains

13:00 – 14:00 Lunch Break

Session V

14:00 – 17:30 **Discussions**

Networking - Joint trip to the Tree Top Adventure Park and subsequent

18:00 Barbecue

Wednesday, 25.09.2019

08:00 – 09:00 Breakfast

09:30 – 12:00 **Postersession**

(coffee break included)

1. ***Alexa Adamkiewicz****:* Tip-Induced Chemical Reactions of Diethyl Ether and Tetrahydrofuran on Si(001)
2. ***Eike Dornsiepen****:* Organotetrelchalcogenide Clusters with Nonlinear Optical Properties
3. ***Tobias Dunaj****:* Interpnictogen Compounds from Diaryl Halido Bismuthanes
4. ***Timo Glaser****:* Azide based functionalization of Si(001)
5. ***Robin Günke*****l**: MOVPE Growth and Characterization of GaAs based W Type Ga(N,As)/Ga(As,Bi)/Ga(N,As) Quantum Well Heterostructures
6. ***Damien Heimes****:* Improved Frozen Lattice Approximation by First Principles Phonon Calculations
7. ***Marcel Köster****:* Sila crown ethers and their coordination towards p-block cations
8. ***Marcel Kröner:*** *Monolithic Integrated Ga(NAsP(Sb)) Laser on Silicon (001)*
9. ***Sven Christian Liebscher****: Ab-initio based calculation of the optical and electronic properties of dilute Ga(SbBi)*
10. ***Oliver Maßmeyer****: Real time mass spectrometric gas phase investigations during MOVPE*
11. ***Bertram Peters****: Ionothermal Approach and Characterization of Telluridomercurates*
12. ***Christian Ritter****: Synthesis and Functionalization of Bis(amido)diazadiarsetidines*
13. ***Luise Rost****: Correlation of optical properties and interface morphology in type- II semiconductor heterostructures*
14. ***Julian Veletas****: Ga(As,Bi) Based W-Type Alloys*
15. ***Maximilian Widemann****: In-situ TEM growth investigations of III/V semiconductor materials*

12:30 – 13:30 Lunch Break

14:00 Departure

Speaker's research summaries

(in order of schedule)

Controlled Manipulation of Diethyl Ether on Si(001) via Tip-Induced Electronic Excitation

Alexa Adamkiewicz[1], Gerson Mette[1], Tamam Bohamud[1], Michael Dürr[1,2], and Ulrich Höfer[1]

[1]*Faculty of Physics and Material Sciences Center, Philipps University, D-35032 Marburg, Germany*
[2]*Institute of Applied Physics, Justus Liebig University Gießen, D-35392 Gießen, Germany*

Introduction

The combination of semiconductor surfaces with organic molecules and their broad range of functionalities could lead to new applications in semiconductor technology, among others, in the fields of optoelectronics, solar cells, or biosensors. In order to control the organic functionalization of semiconductor surfaces, it is important to understand the nature and properties of the adsorption process of the organic molecules on these surfaces. Ultimately, one would like to selectively manipulate the adsorbates in order to induce particular changes in the adsorption configurations and the properties of the adsorbed molecules.

Results

Tetrahydrofuran (THF) and diethyl ether (Et_2O) are used as model systems for the investigation of how to induce and manipulate reactions of organic molecules on silicon via electronic excitation. Thermal activation of the datively bonded intermediate state of THF and Et_2O leads to well defined final configurations in which the molecules or molecular fragments are covalently bound to the surface[1,2]. STM experiments with THF on Si(001) showed that tip-induced excitation of the molecules bound via the intermediate state can open additional reaction pathways resulting in new final configurations. Moreover, it is possible to control the ratio of the different final configurations by means of the applied bias voltage[3]. For Et_2O on Si(001), a qualitatively similar behavior was observed. In particular, a similar threshold value of the bias voltage was deduced for tip-induced electronic excitation and reaction of diethyl ether. On the other hand, the final configurations differ significantly for THF and Et_2O. These differences can be attributed to the different molecular structure of the two molecules. They illustrate how different parameters such as molecular structure on the one hand side and electronic interaction between molecule and surface on the other hand can compete and how this competition influences the transition state and the final products.

Conclusion and Outlook

Tip-induced electronic excitation is thus not only a suitable way to control surface reactions beyond thermal activation, but also allows for a detailed investigation of the driving forces of these reactions. Based on such an in-depth understanding of the adsorption of organic molecules, future projects will focus on the optical functionalization of silicon. In order to understand the electronic properties of organic/inorganic structures at the interface, charge transfer experiments will be performed. A representative model system will be an organic molecule which combines an optically active functional group and cyclooctyne. The latter proved to be a powerful building block in terms of chemoselective adsorption of bifunctional molecules[4,5]. Unlike the vast majority of organic functionalities, which adsorb via a weakly bound intermediate state, cyclooctyne exhibits a direct adsorption pathway[4,6] which controls the adsorption of functionalized cyclooctynes[4,5].

References

[1] G. Mette, M. Reutzel, R. Bartholomäus, S. Laref, R. Tonner, M. Dürr, U. Koert, and U. Höfer, *ChemPhysChem.* **15**, 3725 (2014)

[2] M. Reutzel, G. Mette, P. Stromberger, U. Koert, M. Dürr, and U. Höfer, *J. Phys. Chem. C* **119**, 6018 (2015)

[3] G. Mette, A. Adamkiewicz, M. Reutzel, U. Koert, M. Dürr, and U. Höfer, *Angew. Chem. Int. Edit.* **58**, 3417 (2019)

[4] M. Reutzel, N. Münster, M. Lipponer, C. Länger, U. Höfer, U. Koert, and M. Dürr, *J. Phys. Chem. C* **120**, 26284 (2016)

[5] C. Länger, J. Heep, P. Nikodemiak, T. Bohamud, P. Kirsten, U. Höfer, U. Koert, and M. Dürr, *J. Phys.: Condens. Matter* **31**, 034001 (2019)

[6] G. Mette, M. Dürr, R. Bartholomäus, U. Koert, and U. Höfer, *Chem. Phys. Lett.* **556**, 70 (2013)

Morphological stability analysis of (pseudo-) ternary epitaxial surface

Badal Mondal[1], Andreas Beyer[2] , Kerstin Volz[2], Bruno Eckhardt[1]

[1] *Fachbereich Physik, Philipps-Universität Marburg, Germany*
[2] *Faculty of Physics and Materials Science Center, Philipps-Universität Marburg, Germany*

Introduction

Motivated by the experimental observations on heteroepitaxial growth of III/V ternary and quaternary semiconductor material we analyze the composition effect on surface morphological stability of these type of compounds theoretically. In this context we have studied the thermodynamic as well as the kinetic stability side by side. More specifically, we propose a general theoretical model for (pseudo-ternary) III/V semiconductor compounds of the type $AB_xC_yD_{1-x-y}$ such as Ga(NAsP). Within a mean field approach using 'Delta-Lattice-Parameter (DLP) model'[1] developed in early 1973 by G. B. Stringfellow, we explore the characteristic thermodynamics with and without coherent elastic strain effect given by the lattice model from reference[2], under the appropriate epitaxial growth condition. Concerning kinetics, we investigate the stress-driven coherent island formation due to Stranski-Krastanov growth instability[3] under the assumption of dislocation-free pyramidal-shaped islands and rigid, perfectly flat substrate surface, together with another analogous competitive mechanism of misfit-dislocation formation[4]. And finally we applied our entire theoretical analysis to one of the experimentally well studied III/V quaternary compound Ga(NAsP) under pseudo-ternary approximation.

Results

According to our thermodynamic model the critical temperature (T_c) for Ga(NAsP) grown on GaP comes out to be only 136 ± 1 K; which suggests the system to be fully thermodynamically stable and no sign of phase separation over the entire composition range at and above room temperature.

Using different parameters for the growth of Ga(NAsP) on the (001) surface of GaP the critical thickness from SK-transition $(h_c^{(sk)})$ and also for the misfit-dislocation $(h_c^{(D)})$ had been calculated over the entire composition plane, see fig. 1. Clearly there exists only a small composition region near the $a=a_s$ line where the system can be grown smoothly with a reasonable thickness only. Also as $h_c^{(sk)}\propto 1/\epsilon^2$ but $h_c^{(D)}\propto 1/\epsilon$, where ϵ is the extent of lattice mismatch, they exchange their role depending on ϵ , which in our system turns out to be about 1 %. From the results shown in fig. 1 it is also clear that one can smoothly grow the system with maximum of only ~ 20 % N which has been seen in several experiments so far as well.

Our theoretical analysis shows that to avoid thermodynamic instability (phase separation) one should choose a substrate with lattice parameter near or slightly above the GaP-GaAs end. The kinetic analysis then suggests that shifting $a=a_s$ line towards GaN end increases the N-solubility, as critical thickness develops only near around $a=a_s$ line. Therefore one can easily optimize the lattice parameter for best choice of substrate depending on the system need. For growth of Ga(NAsP) at 800 K, our numerical analysis shows the best choice of substrate will be with the lattice parameter, $a_s\sim 5.1\,\text{Å}$, for the N-solubility of ~ 40-50 % over a

large range of composition, as is shown in fig. 2c. Above this a_s the N-solubility is restricted mainly by h_c (kinetic instability), as is shown in fig. 2a, 2b. Below this value of a_s the thermodynamic instability starts to dominate, as is shown in fig. 2d. Unfortunately as no experimental data for epitaxial growth of Ga(NAsP) on a substrate having lattice constant near $5.1\,\text{Å}$ available so far, this new strategy of substrate optimization is still remain unexplored.

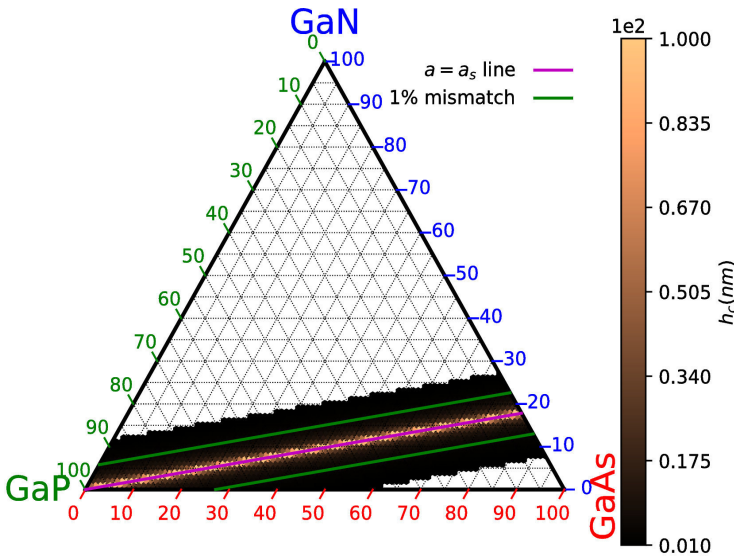

***Figure 1**: Critical thickness for Ga(NAsP) grown on GaP*

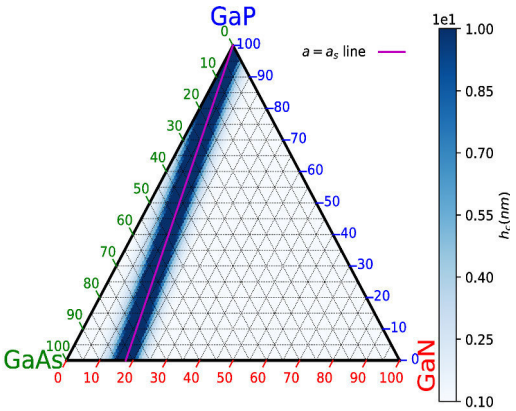

(2a) a_s=5.45 Å

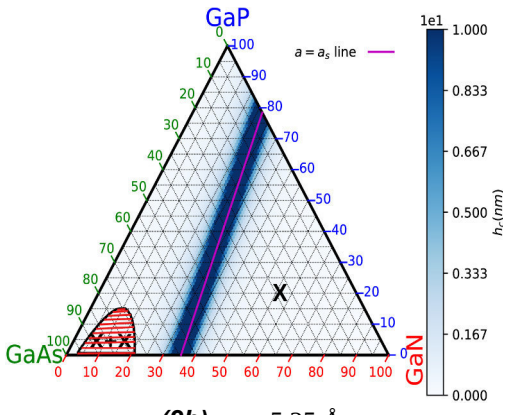

(2b) a_s=5.25 Å

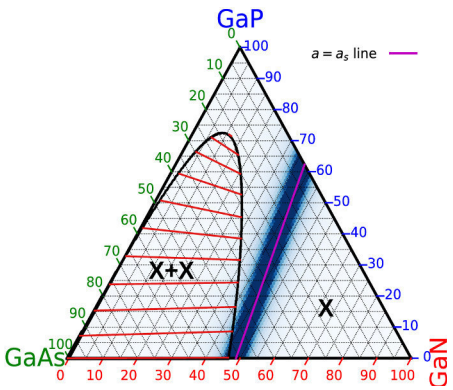

(2c) a_s=5.1 Å

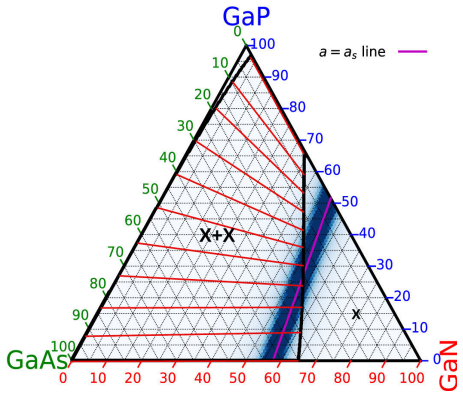

(2d) a_s=5.0 Å

Conclusion

Our theoretical analysis on the surface morphological stability of the quaternary compound Ga(NAsP) under quasi-ternary approximation subject to in plane mismatch strain reveals that, unlike other quaternary compounds, Ga(NAsP) grown on GaP substrate is a *thermodynamically stable* compound over entire composition range which otherwise till date was considered to be 'metastable'. Through kinetic analysis, a critical compressive mismatch strain is predicted, beyond which the epitaxy layer undergoes strain induced instability, forming roughness on a perfectly flat surface or introducing dislocation. We map different regions of stability for this compound considering the combined effect of thermodynamic phase separation and kinetic critical thickness and thereby provide a systematic and consistent way for choosing best substrate-layer pairs. In our particular case the lattice mismatch strain decreases the thermodynamic instability and increases the kinetic instability, such that the combination thereof determine the overall stability. Hence for the full exploitation of heteroepitaxy one requires an extensive understanding of thermodynamic miscibility along with kinetics of strain relaxation as well. We hope that the present theoretical analysis will provide a systematic way for future exploration of other III/V ternary, quaternary compounds as well for the possible means to control the morphology of surface.

Outlook

In order to yield tractable results, we used some simplifying assumptions and limited the scope of our analysis. More specifically, (i) we assumed all islands to be equally sized pyramids with a defined tilt angle, and (ii) our analysis is solely concerned with the dependence of interface roughness on compound composition, and we plan to address these points in the near future. Concerning (i), a complete theoretical explanation for the observed preference of pyramidal shape of the islands is also currently lacking, and in reality islands have size distribution as well. Through extension of our theoretical work we wish to provide a better understanding of these problems. As regards (ii), experimental observations suggest not only composition but temperature also have a significant effect on surface roughness. We are currently working on a model that includes this effect into our calculations in order to understand the underlying physics and to eventually provide predictions. Finally, and most importantly, we wish to quantify how well this analysis performs for systems other than Ga(NAsP), particularly concerning the concept of substrate-optimization developed here.

References

[1] G. B. Stringfellow, "Calculation of ternary and quaternary III–V phase diagrams," *J. Cryst. Growth*, vol. 27, pp. 21–34, 1974.

[2] A. I. Kazakov and I. N. Kishmar, "Stability analysis of quaternary alloys including the lattice mismatch strain energy," *J. Cryst. Growth*, vol. 125, no. 3–4, pp. 509–518, 1992.

[3] D. V. Yurasov and Y. N. Drozdov, "Critical thickness for the Stranski-Krastanov transition treated with the effect of segregation," *Semiconductors*, vol. 42, no. 5, pp. 563–570, 2008.

[4] J. W. Matthews and A. E. Blakeslee, "Defects in epitaxial multilayers: I. Misfit dislocations," *J. Cryst. Growth*, vol. 27, pp. 118–125, 1974.

Automated exploration of reaction networks in chemical vapour deposition by density functional theory

Fabian Pieck, Ralf Tonner

Philipps-Universität Marburg, Faculty of Chemistry, Hans-Meerwein-Straße 4, 35032 Marburg, Germany (Fabian.Pieck@chemie.uni-marburg.de)

The foundation of the present work was laid by studying the gas phase reactivity of precursors used in chemical vapour deposition (CVD). The gas phase decomposition of triethylgallane[1], *tert*-butylphosphine[1], trimethyl- and triethylboron[2] and di-tertiary-butyl-arsano-amine[3] already results in reaction networks spanning more than 60 elementary reactions.

For a detailed understanding of the whole CVD process (Figure 1) a description of the precursor reactivity at the substrate surface is even more important. Unfortunately, an inclusion of a surface in our model system drastically increases it's complexity: Now, for every single adsorption spot all possible decomposition reactions have to be evaluated. Furthermore, new reactions like adsorbate diffusion or reactions with the surface occur. From a technical point of view, the computational effort rises significantly by considering the surface since now an extended slab model has to be applied. Thus, density functional theory remains as the only viable workhorse.

Our present work aims at obtaining the decomposition network of CVD precursors at the substrate surface by tackling the stated problems. The general idea here comprises two pillars: On the one hand the time-consuming step of manually searching for multiple reaction pathways is replaced by a systematic and automated procedure. This enables us to manage the high total number of reaction paths, while the possibility to miss an important reaction channel is reduced. On the other hand we utilize the Message Passing Interface (MPI) protocol to efficiently parallelize our code to make it useable on national supercomputer facilities. This parallelization does not reduce the computational effort as such but spreads the workload over many compute notes. In this way the real time (wallclock time) to solve a computational problem is drastically reduced. Overall, we are aiming at calculating the reaction networks at modern high performance computers using tens of thousands cores at once.

The automated approach itself consists of three main steps: In a first step, every decomposition product is created. This is achieved by using a simple distance criterium to identify bonded atoms in the precursor. The knowledge of the bonds enables the code to manipulate (breaking, rearranging) them. In this way important types of reactions like homolytic fission of bonds, α- and β-H-eleminations are described. In a second step, every structure is separately placed on a grid, which equally divides the surface. The structures are optimized to obtain the minima on the potential energy surface consisting of the adsorption structures. In a third step, the reaction paths connecting two of the previously obtained minima are selected and calculated by the nudged elastic band method.

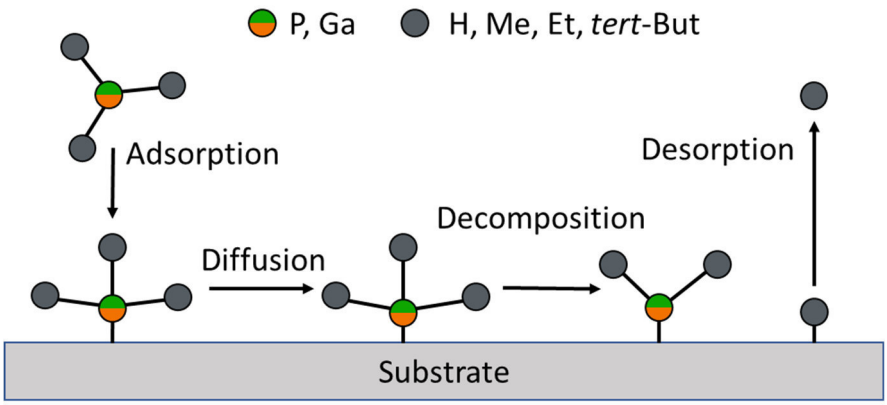

Figure 1: *Schematic overview of the elemental steps in chemical vapor deposition. The reaction network consists of energetic minima (structures) and reaction paths connecting the minima (arrows).*

The individual steps of the algorithm are tested and debugged using gallane (GaH_3) on GaP(001). Once every part of the code is optimized, the decomposition of trimethylgallium ($Ga(CH_3)_3$) on a GaP(001) surface is studied as a real test system. In the future, we also want to expand the code to study reaction networks for atomic layer deposition (ALD). The growth of layered transition metal dichalcogenides like MoS_2 is a notable example.

[1] A. Stegmüller, P. Rosenow, R. Tonner, *Phys. Chem. Chem. Phys.* **2014**, 16, 17018-17029.

[2] a) M. Imam, K. Gaul, A. Stegmüller, C. Höglund, J. Jensen, L. Hultman, J. Birch, R. Tonner, H. Pedersen, *J. Mater. Chem. C* **2015**, 3, 10898 – 10906; b) M. Imam, L. Souqui, J. Herritsch, A. Stegmüller, C. Höglund S. Schmidt, R. Hall-Wilton, H. Högberg, J. Birch, R. Tonner, H. Pedersen, *J. Phys. Chem. C*, **2017**, 121, 26465-26471.

[3] E. Sterzer, A. Beyer, L. Duschek, L. Nattermann, B. Ringler, B. Leube, A. Stegmüller, R. Tonner, C. von Hänisch, W. Stolz, K. Volz*, J. Cryst. Growth*, **2016**, 439, 19-27.

Optical Spectroscopy of Ga(NAs)/Si and (GaIn)As/GaAs/Ga(AsSb) heterostructures

Luise Rost, Khushboo Patel, Sebastian Gies, Peter Ludewig, Wolfgang Stolz and Wolfram Heimbrodt

Department of Physics and Material Sciences Center, Philipps-Universität Marburg

Introduction

Infra-red semiconductor lasers for long-range optical communication using optical fibers are still a highly topical field. There are many ways to achieve long wavelength lasing in the range of 1.3 µm. We present here two different approaches to reach longer wavelength with III-V semiconductors.

A strategy to get to longer wavelength and to overcome Auger losses is the use of type-II devices, where the recombining electrons and holes are spatially separated[1,2]. Additionally, such systems offer more degrees of freedom for device design as the band edges of the electron and the hole confining wells can be varied independently allowing for a wide tuning of the type-II transition energy. A promising heterostructure design for such applications are so called W-laser structures, which enable the optimization of the wave function overlap by adding barrier layers to confine carriers. With the continuing progress of device miniaturization in mind, the properties of the internal interfaces are getting more and more important. In this study, we present as thorough investigation of photoluminescence properties of (Ga,In)As/GaAs/Ga(As,Sb) heterostructures with modified interface morphology.

Dilute Nitride Semiconductors have been of great research interest since their development in the 1990s, both, because of their unique physical properties and potential device applications. The substitution of small amounts of nitrogen atoms with group V elements in conventional III–V semiconductors such as GaAs or GaP strongly affects their electronic structure and allows one to tailor the band structure of the III–V semiconductors[3-5]. In this work we investigate the photoluminescence properties of GaNAs quantum wells on silicon with N concentration between 6,9 % and 16,9 %.[6]

Results

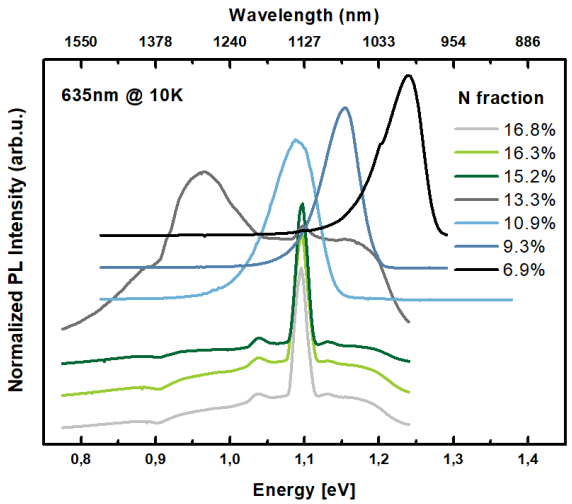

Figure 1: *Low temperature photoluminescence of GaNAs/GaP/Si with increasing N concentration.*

We could show that a Photoluminescence (PL) signal is possible to detect at cryogenic temperatures from a GaNAs quantum well up to 13 % of N incorporation. A red shift up to 1,3 µm could be found, but the PL intensity decreases with rising N concentration. For concentrations over 13 % only a signal from the GaP/Si substrate was observable. With temperature depending photo-luminescence measurements we could reveal that the disorder behavior is not linear to the increasing N concentration.

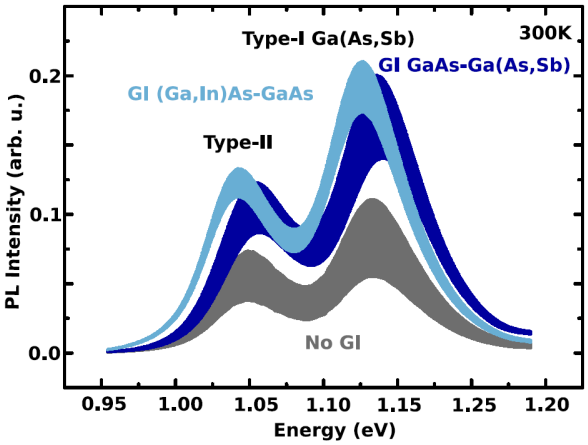

Figure 2: *Mean photoluminescence of the (Ga,In)As/GaAs/Ga(As,Sb) heterostructures taken at six different spatial positions.*

The (Ga,In)As/GaAs/Ga(As,Sb) heterostructures were grown by metal-organic vapor-phase epitaxy. A modification of the interface morphology was introduced by a growth interruption (GI) for 120s at different interfaces between the GaAs barrier and the active quantum wells. To correlate the structural changes with the optical properties we investigated the cw-PL. We could clearly show that a growth interruption of 120s at the interfaces of the type II quantum wells increases the PL intensity and type II recombination time, because of smoother interfaces.

Outlook: what is planned

In both cases we like to do further investigation. For the GaNAs heterostructure we will compare the experimental data with theoretical QW-calculations including the band anticrossing model. Furthermore, it is planned to measure the absorption bands by photo modulated reflectance spectroscopy.

For the type II (Ga,In)As/GaAs/Ga(As,Sb) heterostructure we want to investigate the reason for the odd time resolved photoluminescence behavior at 10 K (see Fig. 3). For that, we will establish a kinetic model and work together with the theory group of Prof. S. W. Koch on a fully microscopic description.

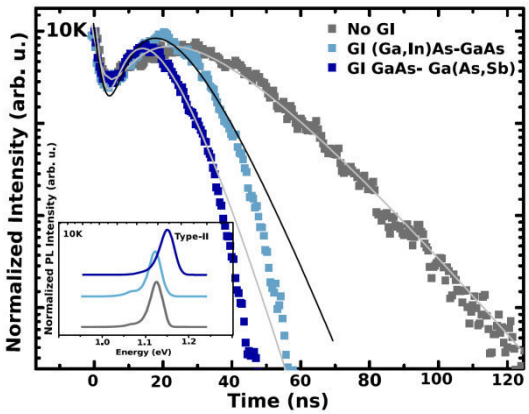

Figure 3: *Transients of the type-II PL at 10 K. The curves are normalized to unity and were taken at the maximum of the type-II peak. The inset shows the normalized cw-PL at 10 K.*

References

[1] Berger, C. et al., AIP Adv. 5, 047105 (2015).
[2] Gies, S. et al., Appl. Phys. Lett. 107, 182104 (2015).
[3] Kunert, B. et al., Appl. Phys. Lett. 88, 182108 (2006).
[4] Kunert, B. et al., phys. stat. sol. (b) 244, 2730 (2007).
[5] Volz, K. et al., J. Cryst. Growth 315, 37 (2011).
[6] Ludewig, P. et al., J. Cryst. Growth, *467*, 61–64 (2017).

Optoelectronic Coupling between Colloidal Quantum Dots and Semiconductor Substrates

Mikko Wilhelm and Wolfram Heimbrodt

Faculty of Physics, Philipps-Universität Marburg

Introduction

The optoelectronic interaction between colloidal II-VI semiconductor quantum dots (QDs) and different semiconductor substrates is studied. The QDs synthesized from solutions are deposited on the semiconductor surfaces and linked via Van der Waals interaction to the substrate. Such hybrids are promising systems for applications as gas sensors, photo sensors or solar cells. The aim is to investigate and describe the interaction between the QDs and semiconductor substrates.

Results

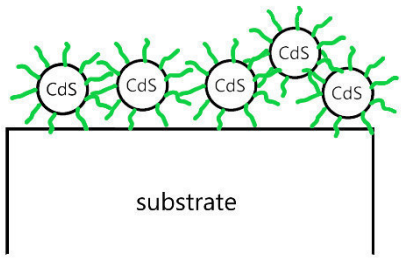

Colloidal CdS quantum dots with and without a ZnS shell were deposited from toluene solution on the semiconductor substrates via knife coating in order to achieve a thin quantum dot layer with little solution wasting. For many measurements MBE grown ZnSe/ZnMnSe quantum well structures were used as substrates ($E_g \approx 2.8$ eV at 10 K). The different quantum dot samples differ mainly in their size and thus bandgap energy (Eg ≈ 2.5 eV - 3.1 eV at 10 K). Optical characterization of the coupled samples was carried out using time resolved and continuous wave photoluminescence spectroscopy at different temperatures. In the case of a thick QD layer no change in the PL decay properties of the QDs could be observed compared to the QDs deposited on SiO_2. But depending on the substrate, the QD PL decay time is different in the case of a thin QD layer. The PL intensity and decay time of QDs with a higher band gap decreases when the quantum dots are deposited on ZnSe, but the effect is smaller when the substrate is doped with Mn. The QDs with a lower energy show a different change in their PL decay time.

Conclusion and Outlook

The interaction between the colloidal QDs and the substrate is weak, but the slight change in the PL decay time indicates an energy or charge transfer. The additional doping of ZnSe with Mn hardly changes the band gap of substrate, but the different band alignment of the substrate causes a change in the PL behavior of deposited QDs. The theoretical models to describe the behavior should be expanded and additional measurements be performed (Raman, magnetic field and temperature dependent PL measurements) in order to gain a deeper understanding of the underlying physical processes.

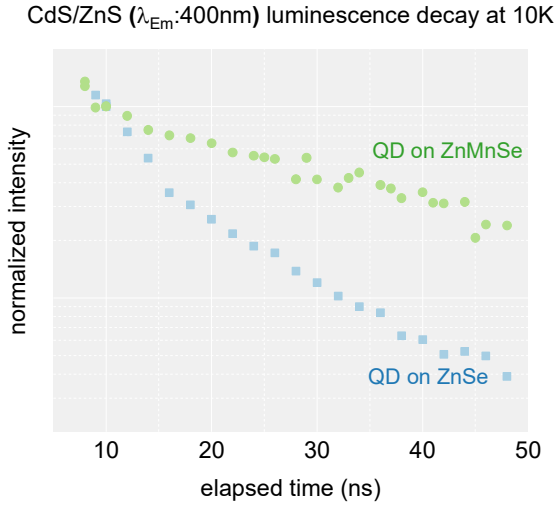

Figure 1: *Luminescence decay of Quantum Dots on different substrate. The PL decay changes with the substrate*

Investigation of Coherent Interface Phonons in GaP/Si Heterostructures by Means of Pump-Probe Differential Reflection

Steven Youngkin[1], Gerson Mette[1]

[1]*Fachbereich Physik und Zentrum für Materialwissenschaften Philipps-Universität, D-35032 Marburg*

Introduction

GaP and Si have a lattice mismatch of less than 0.4 %, making thin films of GaP, which are epitaxially grown on Si, a model III-V on Si (polar on non-polar) semiconductor heterostructure system. The goal of our work is to understand the elementary light-induced excitations at the GaP/Si interface. These include electronic transitions and the subsequent charge transfer into the Si bulk system or GaP thin film layer. Previous studies using time-resolved second harmonic generation have shown the existence of an electronic interface state which lies energetically in the band gap of both materials. Electrons excited via this interface state are efficiently injected into the conduction band of Si and wavelength dependent measurements exhibit a resonant excitation at energies of around 1.4 eV.[1]

By means of coherent phonon spectroscopy, bulk phonon modes in GaP and Si, phonon-plasmon coupled modes in the heterostructure, and acoustic pulses generated at the interface, have been observed for the GaP/Si heterostructures.[2-4]

In our experiments, we use a tunable laser for our pump beam, and a single-color probe beam for the detection of such elementary excitations. By observing changes in the reflection of the probe beam from the GaP/Si sample, after excitation by the pump beam, we can directly observe the pump-induced dynamics with a time-resolution in the femtosecond regime.

Results

Fig. 1 illustrates an example of a pump-probe differential reflection measurement using an excitation energy above the indirect band gap of Si (1.12 eV), but still far below the band gap energy of GaP (2.26 eV). As reference, in bulk Si (blue curve) there is an initial spike in the normalized differential reflection, which is due essentially to the cross-correlation of the pump and probe pulse, followed by a step-like decrease and a long-living recovery. In comparison, the signal from the 10 nm GaP/Si heterostructure exhibits a far more complex behavior. Like in Si, there is a rapid decrease in the transient, but it is followed by a much faster recovery. We associate this complex behavior of the transient to underlying carrier excitations and charge transfer away from the interface. Most important is the observation of a coherent phonon in the differential reflection. By fitting the overall transient at positive pump-probe

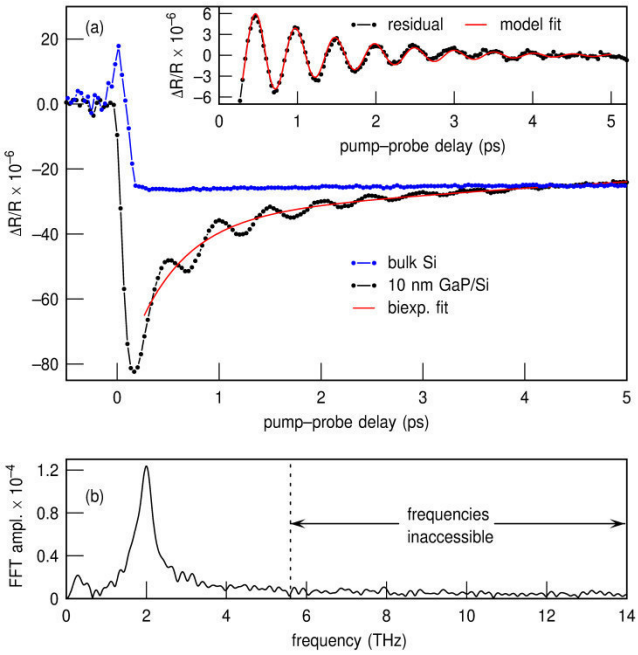

Figure 1: *Example of data obtained by means of time-resolved pump-probe differential reflection in 10 nm GaP/Si. (a) Comparison between the measured transients between bulk Si and GaP/Si. A coherent oscillation is clearly visible after photoexcitation by the laser source (see inset). (b) FFT of the residual reveals a phonon mode with a frequency centered around 2 THz. The current pulse duration limits the accessible frequencies.*

delays with a biexponential function and subtracting it from the data, we obtain the residual comprised solely of the oscillatory component (see inset in Fig. 1 (a)). We model the oscillation as a damped periodic function. From this we can obtain the amplitude, frequency, dephasing rate, and phase shift of the coherent phonon mode. Fig. 1 (b) shows the FFT of the residual, revealing that the observed coherent phonon mode has a center frequency around 2 THz. We do not observe bulk phonon modes in Si or GaP with that frequency. Therefore, this suggests that the 2 THz phonon mode arises due to the semiconductor interface.

Furthermore, we conducted wavelength dependent measurements to probe how the amplitude of the 2 THz mode is related to the interface electronic resonance centered around 1.4 eV (885 nm) which was previously observed by means of time-resolved second-harmonic generation.[1] Indeed, we observe an oscillation and an electronic response even at wavelengths beyond the absorption edge in silicon (roughly at 1100 nm). The amplitude of the 2 THz mode also exhibits a similar resonant behavior around 885 nm. This seems to suggest a complex interaction at the interface between the resonantly excited electronic system and the amplitude of the interface vibrational mode. Our investigations are not limited to the 10 nm GaP/Si heterostructure. We also observe this 2 THz mode in thicker samples up to 48 nm but with lower amplitudes. The resonant behavior of the amplitude has also been observed in our thickest sample of 48 nm.

Conclusion

The leading interpretation so far regarding the origin of the 2 THz interface phonon mode involves the combination of two bulk phonon modes likely originating in both Si and GaP bulk systems. Unfortunately, our current setup is incapable of resolving higher frequency phonon modes due to the long pulse duration (around 60 fs). Fig. 1 (b) illustrates the region in which some of the bulk modes could be seen in the FFT but are currently inaccessible. Having a broader range in our FFT spectrum will allow us to observe the properties of the bulk phonon modes and any correlation they may have with the 2 THz, or any other, interface phonon mode.

Outlook

We are currently building a new optical setup at a new laser system which provides tuneable laser pulses with pulse durations less than 30 fs, allowing us to resolve a much greater range of accessible frequencies. Furthermore, second harmonic generation detection will be incorporated into our coherent phonon spectroscopy setup, since SHG is a more interface sensitive probing technique. All of this will allow us to make greater strides in our investigation of coherent interface phonons in the model system of GaP thin films grown on Si.

References

[1] G. Mette et al., in preparation.
[2] K. Ishioka et al., Appl. Phys. Lett. **108**, 051607 (2016).
[3] K. Ishioka et al., Appl. Phys. Lett. **111**, 062105 (2017).
[4] K. Ishioka et al., J. Phys.: Condens. Matter **31**, 094003 (2019).

Organotetrel Chalcogenide Clusters with Nonlinear Optical Properties

Eike Dornsiepen and Stefanie Dehnen*

Faculty of Chemistry and Material Sciences Center, Philipps-Universität Marburg

Tetrelchalcogenide clusters featuring organic ligands have attracted increasing attention during recent years due to their intriguing chemical and physical properties.[1] The organic ligands influence their optical properties as well as their reactivity towards molecules and surfaces.[2] Recent investigations on the organotin sulfide cluster $[(StySn)_4S_6]$ featuring an adamantane-like topology have demonstrated extreme optical nonlinearity, allowing for white light emission when driven by an IR laser diode.[3]

Based on this result, the white light generation (WLG) initially observed on $[(StySn)_4S_6]$ was investigated in more detail. For this purpose, the substance library was significantly extended, in particular in order to analyze necessary prerequisites for the white-light emission. By systematic variation of both the core composition and the organic substituents the understanding of the underlying mechanism was improved, and possible ways to selectively modify the emission spectra were found. In a first study, it could be shown by varying the tetrel element and the substituents that the amorphicity of the compounds is a basic requirement for the WLG, since otherwise emission occurs in phase as second harmonic generation (SHG).[4] By further variation of the organic substituents and replacement of the sulfur atoms in the inorganic core by selenium atoms, it was further found that - opposing the initial hypothesis - no π electron system, but only a cyclic organic substituent is required, and that the emission seems to be limited by the HOMO-LUMO gap of the compound.[5]

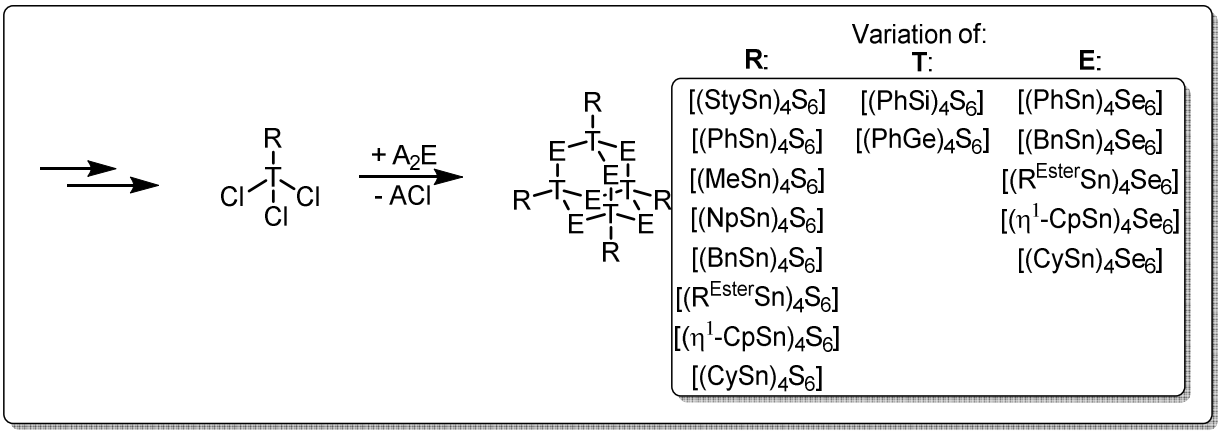

Figure 1: *Substance library of adamantane-type $[(RT)_4E_6]$ clusters investigated with respect to their optical properties.*

In a second project, the reactivity of $[(PhSn)_4S_6]$ towards transition metal complexes was investigated, whereby different ternary clusters were obtained. In reactions with coinage metal complexes with sterically less demanding phosphine ligands, clusters were synthesized in which the inorganic core of the starting material is retained and one of the phenyl substituents is replaced with a coinage metal complex fragment. The resulting clusters have the composition $[\{(R_3P)_3MSn\}\{PhSn\}_3S_6]$ (M/R = Cu/Me, Ag/Et, Au/Me).[6] However, by use of the more bulky phosphine ligand PPh_3 the organotin sulfide cluster is decomposed and subsequently rearranged to a larger ternary cluster with the composition $[(CuPPh_3)_4(PhSn)_{18}Cu_6S_{31}Cl_2]$, which is the first cluster with ternary inorganic core which was obtained without an additional source of sulfide.[7]

Transferring the ligand-exchange reactions carried out with coinage metal complexes to Group 6 complexes allowed for the preparation of clusters with the composition $[\{(PhSn)_3SnS_6\}\{(CpM)_3S_4\}]$ (M = Mo, W) in which an adamantane-type organotinsulfide cluster is substituted with a thiotungstate or thiomolybdate cage. The thiometalate cages correspond to sections of a MoS_2 or WS_2 layer, which allows the compounds to be considered as molecular model systems for the adsorption of organotin sulfide clusters on corresponding surfaces. The binding situation in the molecules was rationalized by DFT calculations, which revealed a mixed-valence situation and an unusual two-electron-four center bond connecting the two subunits of the molecules. DFT calculations with periodic boundary conditions showed these systems to be molecular models for the adsorption of organotin chalcogenide clusters on a MoS_2 or WS_2 surface, given suitable doping of the TMDC surface.[8]

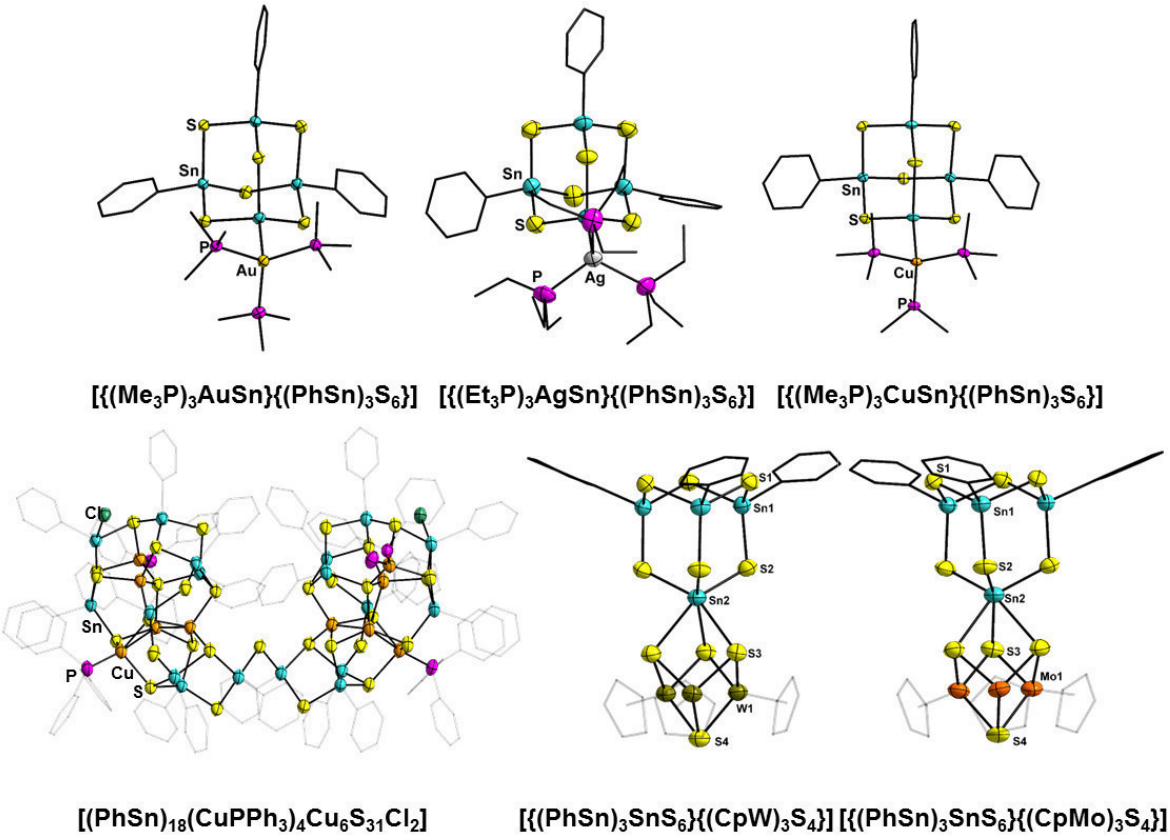

$[\{(Me_3P)_3AuSn\}\{(PhSn)_3S_6\}]$ $[\{(Et_3P)_3AgSn\}\{(PhSn)_3S_6\}]$ $[\{(Me_3P)_3CuSn\}\{(PhSn)_3S_6\}]$

$[(PhSn)_{18}(CuPPh_3)_4Cu_6S_{31}Cl_2]$ $[\{(PhSn)_3SnS_6\}\{(CpW)_3S_4\}]$ $[\{(PhSn)_3SnS_6\}\{(CpMo)_3S_4\}]$

Figure 2: *Overview of the prepared ternary cluster compounds.*

References

[1] a) H. Berwe, A. Haas, *Chem. Ber.* **1987**, *120*, 1175; b) Z. Hassanzadeh Fard, C. Müller, T. Harmening, R. Pöttgen, S. Dehnen, *Angew. Chem.* **2009**, *121*, 4507.

[2] E. Leusmann, F. Schneck, S. Dehnen, *Organometallics* **2015**, *34*, 3264.

[3] N. W. Rosemann, J. P. Eußner, A. Beyer, S. W. Koch, K. Volz, S. Dehnen, S. Chatterjee, *Science* **2016**, *352*, 1301.

[4] N. W. Rosemann, J. P. Eußner, E. Dornsiepen, S. Chatterjee, S. Dehnen, *J. Am. Chem. Soc.* **2016**, *138*, 16224.

[5] E. Dornsiepen, F. Dobener, S. Chatterjee, S. Dehnen, **2019**, *submitted*.

[6] E. Dornsiepen, F. Dobener, N. Mengel, O. Lenchuk, C. Dues, S. Sanna, D. Mollenhauer, S. Chatterjee, S. Dehnen, *Adv. Opt. Mater.* **2019**, *7*, 1801793.

[7] E. Dornsiepen, F. Weigend, S. Dehnen, *Chem. Eur. J.* **2019**, *25*, 2486.

[8] E. Dornsiepen, F. Pieck, R. Tonner, S. Dehnen, *manuscript in preparation*.

MOVPE Growth of Ga(N,As)/Ga(As,Bi)/Ga(N,As) W Type Structures

Thilo Hepp[1,*], Julian Veletas[2], Robin Günkel[1], Oliver Maßmeyer[1], Johannes Glowatzki[1], Sangam Chatterjee[2] and Kerstin Volz[1]

[1]Material Sciences Center and Department of Physics, Philipps Universität Marburg,
[2]Institute of Experimental Physics I, Justus-Liebig-Universität Gießen
**thilo.hepp@physik.uni-marburg.de*

In this work we will present the growth of Ga(N,As)/Ga(As,Bi)/Ga(N,As) W Type structures grown on GaAs in terms of their growth properties and photoluminescence (PL). These structures can be grown strain balanced on GaAs, since Ga(As,Bi) is compressively strained while Ga(N,As) is tensile strained. Due to the strong reduction of the band gap by incorporation of nitrogen (N) and bismuth (Bi) respectively, it is possible to shift the emission wavelength of such structures into the mid infrared region for application as telecom lasers.[1]

The samples were grown in an Aixtron AIX 200 horizontal reactor system. Since deposition of Ga(As,Bi) requires low growth temperatures around 400 °C, triethylgallium (TEGa), tertiary-butylarsine (TBAs) and trimethylbismuth (TMBi) were chosen as precursors. For incorporation of N into GaAs 1,1-dimethylhydrazine (UDMHy) was used. The layer thicknesses and compositions were determined using high resolution X-Ray diffraction (HR-XRD). A frequency doubled Nd:YAG laser was used for excitation of the samples to record the PL signal. The sample surface was investigated using an atomic force microscope (AFM).

Fig. 1 a) shows an HR-XRD diffractogram of a Ga(N,As)/Ga(As,Bi)/Ga(N,As) W Type structure. The clear appearance of pendellösung fringes coupled with good agreement between dynamic modelling and experimental data suggests abrupt interfaces between the different material systems. The inset shows the desired sample structure.

The corresponding PL spectrum of this sample is shown in Fig. 1 b) together with the PL spectra of test structures consisting of three Ga(N,As) and Ga(As,Bi) quantum wells, respectively. The PL peak of the W Type structure is clearly red shifted compared to the PL peak of both test structures, as expected for a Type II transition.

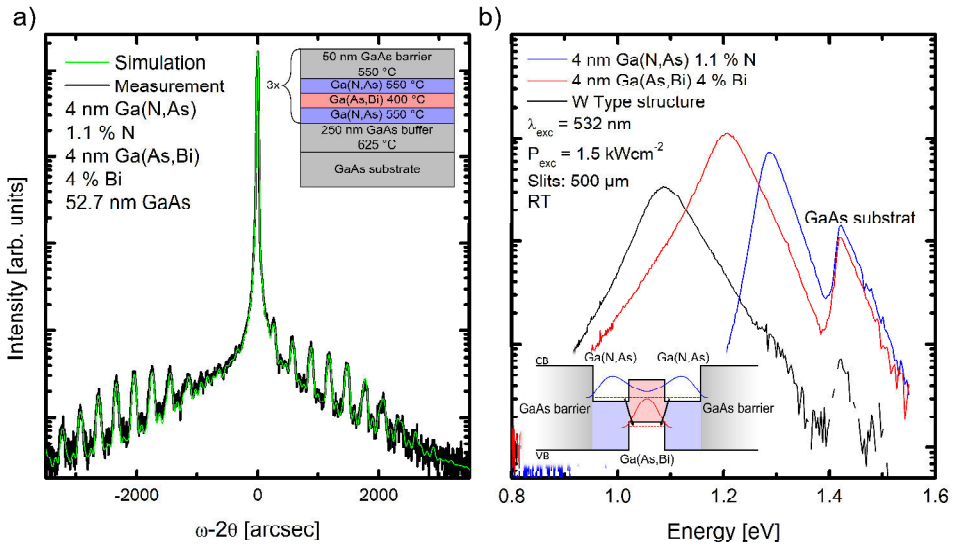

Figure 1: *a) shows an HR-XRD of a Ga(N,As)/Ga(As,Bi)/Ga(N,As) W Type structure. The inset sketches the sample structure. b) shows the PL spectra of the W Type structure as well as the Ga(N,As) and Ga(As,Bi) test structures, respectively. The resulting band structure without strain is depicted as inset.*

[1] C. A. Broderick et al, Sci. Rep. **7**, 46371 (2017).

Nitrogen incorporation in GaP on Si using novel metal organic N-P precursor di-*tert*-butyl-amino-phosphan (DTBAP)

J. Glowatzki[1], O. Maßmeyer[1], M. Köster[2], C. von Hänisch[2], W. Stolz[1], K. Volz[1]

[1]*Faculty of Physics and Materials Science Center - Philipps University Marburg*
[2]*Faculty of Chemistry and Materials Science Center - Philipps University Marburg*

Introduction

GaP based dilute nitrides like $Ga(N_xP_{1-x})$ and $Ga(N_xAs_yP_{1-x-y})$ are discussed in the context of solar cell and laser applications especially on Si [1-2].

The novel precursor di-*tert*-butyl-amino-arsan (DTBAA) shows a high incorporation of nitrogen during growth of $Ga(N_xAs_{1-x})$[3], $(Ga_{1-y}In_y)(N_xAs_{1-x})$[4] and $Ga(N_xAs_{1-x-y}Sb_y)$[5] and no additional arsenic precursor is needed. Due to this advantages a similar precursor with phosphorus instead of arsenic was synthesized. This precursor is the di-*tert*-butyl-amino-phosphan (DTBAP; structure shown in fig.1). Metal organic vapor phase epitaxy (MOVPE) growth experiments took place in an Aixtron Aix 200 horizontal reactor with gas foil rotation and the samples were analyzed by high resolution X-ray diffraction (HRXRD) and atomic force microscopy (AFM) measurements.

$Ga(N_xP_{1-x})$ growth with DTBPA on Si and GaP

The nitrogen incorporation, growth rate and surface morphology were investigated for different growth temperatures as well as different TEGa, TBP and DTBAP partial pressures. Samples were grown on an exact (001) Si substrate with a GaP nucleation layer. It was possible to grow $Ga(N_xP_{1-x})$ in good structural layers without using additional TBP as phosphorus source. This was confirmed by the good agreement between HRXRD measurements and dynamic simulations. Therefore, DTBAP supplies nitrogen and phosphorus simultaneously.

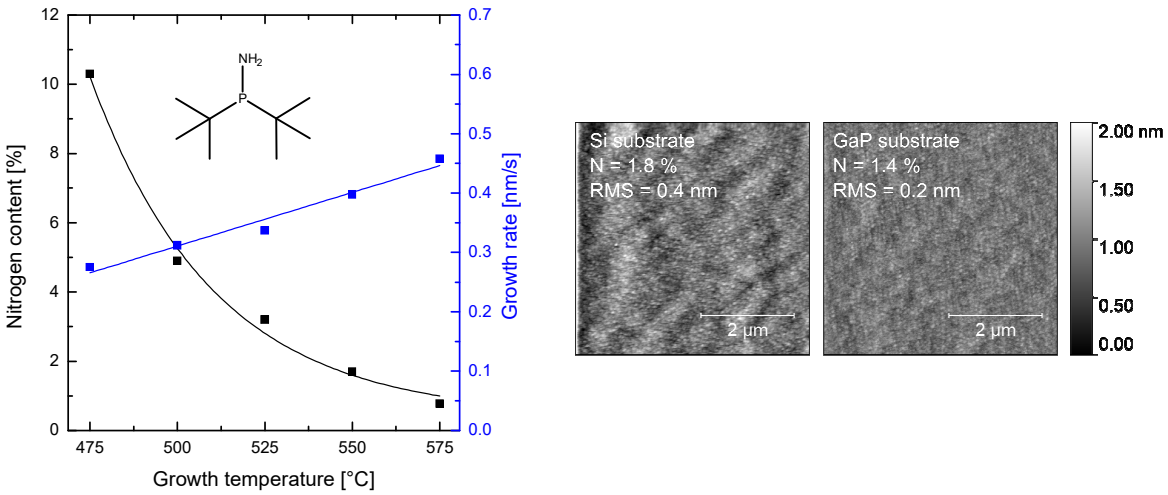

Figure 1: *Left: Inlet shows structure of DTBPA. Nitrogen content and growth rate of $Ga(N_xP_{1-x})$ are plotted in dependence of growth temperature. P_p(TEGa) = 7.1E-3 mbar; P_p(DTBAP) = 2.6E-2 mbar. Right: AFM images of samples grown under same conditions (P_p(TEGa) = 7.1E-3 mbar; P_p(DTBAP) = 1.9E-2 mbar; T_{gr} = 525 °C) on Si and GaP substrates.*

In fig. 1 the nitrogen content and the growth rate are plotted vs. the growth temperature. The other parameters were kept constant during growth. One can see an increasing growth rate due to the higher decomposition of the TEGa and an exponentially decrease of the nitrogen content with increasing temperature. This behavior was also observed for the conventional nitrogen precursor UDMHy[6]. A Maximum nitrogen incorporation of about 10 % was reached at a growth temperature of 475 °C. Growth experiments with additional supply of TBP together with the DTBAP led to a strong decrease of the nitrogen incorporation which is believed to be caused by the competition for the group V lattice sites between phosphorus and nitrogen.

In comparison to the growth on GaP on Si few samples were grown on GaP substrates under the same growth conditions to investigate the influence of different substrates. Two AFM measurements are shown in fig. 1 on the right.

The effects of the variation of other growth parameters and results of the AFM measurements will be discussed in the presentation.

References

[1] S. Sukittanon et al., Appl. Phys. Lett. **107**, 153901 (2015)
[2] B. Kunert et al., phys. stat. sol. (c) **3**, No. 3, 614–618 (2006)
[3] E. Sterzer et al., J. Cryst. Growth, **439** (19-27) (2016)
[4] E. Sterzer et al., J. Cryst. Growth, **467** (132-136) (2017)
[5] E. Sterzer et al., AIP Advances **8**, 055329 (2018)
[6] B. Kunert et al., J. Cryst. Growth, **272** (753-759) (2004)

Optimization of Ga(N,As,Sb)/(B,Ga)(As,P)-heterostructures for laser applications on Si (001) substrate

M. Kröner, P. Ludewig, J. Zimmet, S. Reinhard, M. Volk, W. Stolz

Faculty of Physics and Material Sciences Center, Philipps-Universität Marburg, Germany

Introduction

One of the big challenges in Si based optoelectronics (OEIC) is the realization of a stable and efficient laser integrated on exact Si (001) substrate. The goal of this project is the pseudomorphical deposition of Ga(N,As)/(B,Ga)(As,P)-quantum well heterostructures by metal organic vapour phase epitaxy (MOVPE) with very low defect densities. While the lower interface of the Ga(N,As)-quantum well is very abrupt, a roughening of the upper interface is detected in STEM studies[1]. When incorporating high amounts of 7 % - 17 % of N into the quantum well material Ga(N,As) it is observed in current STEM studies that defects form at its upper interface propagating through the (B,Ga)(As,P)-cap layer up to the samples surface, leading to three dimensional platelet growth[2]. The density and height of these platelets can be investigated using atomic force microscopy (AFM). Optical properties are investigated by photoluminescence spectroscopy (PL), structural and compositional analysis is carried out by means of high resolution X-ray diffraction (HR-XRD).

Results

In order to improve the quantum wells upper interface quality several growth conditions have been varied. A very promising approach is the addition of Sb during quantum well growth. Sb acts as a surfactant reducing the surface diffusion length which helps growing highly strained materials like the investigated Ga(N,As,Sb) on Si (001)[3]. AFM analysis reveals a clear reduction of the (B,Ga)(As,P)-cap roughness due to the reduction of the platelet density and size indicating a strong reduction of the defect density at the quantum wells upper interface. Growth studies have been carried out varying the partial pressure ratio of Sb/Ga from 0 to 0.12 with a fixed N content in the quantum well of about 9.5 %, as well as varying the N content from 7.4 % to 13.1 % while keeping a fixed Sb/Ga-ratio of 0.06. HR-XRD analyses reveal good interfacial quality for the higher Sb/Ga-ratios. The emission wavelengths for these different N contents range from 1000 nm to 1120 nm (Figure 2). The AFM analysis shows the lowest roughness for the Sb/Ga-ratio of 0.06 to be obtained for N contents higher than 11 % (Figure 1). For fixed amounts of N around 9.5 % the lowest roughness of the overgrown (B,Ga)(As,P)-cap is obtained for the Sb/Ga-ratio of 0.09.

Conclusions & Outlook

The presented data leads to the conclusion that the addition of Sb during Ga(N,As,Sb) growth significantly reduces the defect formation at the quantum wells upper interface as indicated by AFM analysis of Ga(N,As,Sb)/(B,Ga)(As,P)-quantum well heterostructures. For the presented experiments it is expected that no significant amount of Sb is incorporated into the quantum well material and that Sb mainly acts as a surfactant during growth. In future experiments the fraction of Sb in Ga(N,As,Sb) will be increased in order to approach emission wavelengths as long as 1.3 µm.

References

[1] P. Ludewig, S. Reinhard, K. Jandieri, T. Wegele, A. Beyer, L. Tapfer, K. Volz and W. Stolz, “MOVPE growth studies of Ga(NAsP)/(BGa)(AsP) multi quantum well heterostructures (MQWH) for the monolithic integration of laser structures on (001) Si-substrates“, J. Cryst. Growth 438, 63-69 (2016).

[2] P. Ludewig, M. Diederich, K. Jandieri and W. Stolz, “Growth of high N containing GaNAs/GaP/BGaAsP multi quantum well structures on Si (001) substrates“, J. Cryst. Growth 467, 61-64 (2017).

[3] J. Massies and N. Grandjean, “Surfactant effect on the surface diffusion length in epitaxial growth”, Phys. Rev. B 48, 11 (1993).

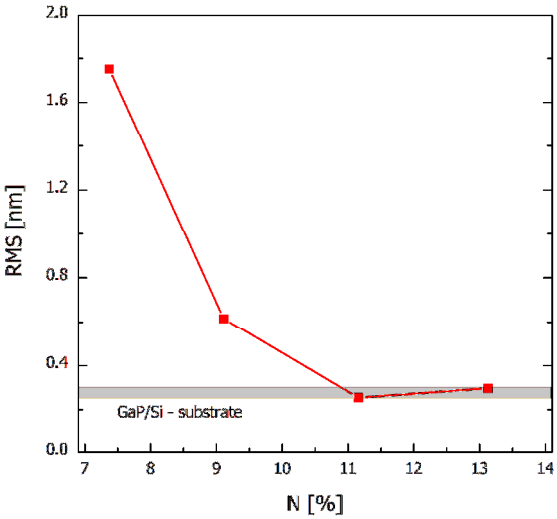

Figure 1: *Surface roughness as root mean square (RMS) from AFM measurements of the (B,Ga)(As,P)-cap on the Ga(N,As,Sb) quantum well for different N-fractions.*

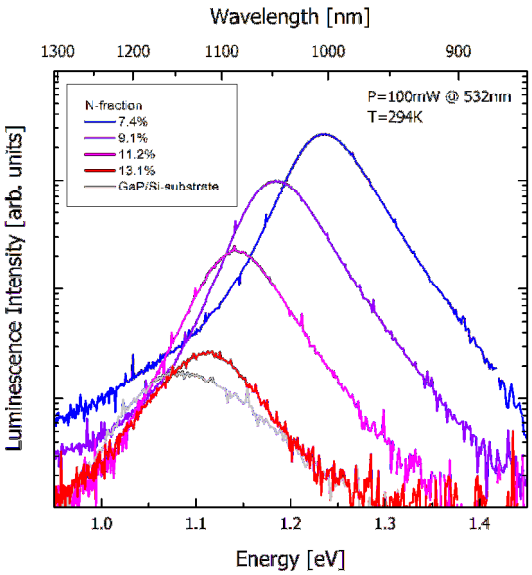

Figure 2: *PL spectra of Ga(N,As,Sb)/(B,Ga)(As,P) - quantum well heterostructures at room temperature for different N-fractions.*

Decomposition Analysis of TBAs and TBP during GaAs and GaP Growth by MOVPE

O. Maßmeyer*, J. Glowatzki, T. Hepp, W. Stolz, K. Volz

Faculty of Physics and Materials Sciences Center, Philipps-Universität Marburg
**oliver.massmeyer@physik.uni-marburg.de*

Introduction

Metal-organic vapor phase epitaxy (MOVPE) is a well-established commercial production technique for many kinds of electronic and photonic devices, such as LEDs, laser diodes, solar cells, high electron mobility transistors, integrated circuits, and many more.[1] To realize these devices by MOVPE the choice of the right metal organic precursor is required to achieve the desired material compositions and purity. Especially for the fabrication of meta stable alloys based on III/V semiconductors like e. g. Ga(N,As) or Ga(As,Bi) the growth temperature has to be quiet low (T < 550 °C) compared to the standard MOVPE conditions (T > 600 °C). Therefore, the chosen precursors need to be fully decomposed below these temperatures.

In this work the general influence of the Ga precursors trimethylgallium (TMGa), triethylgallium (TEGa) and tri-*tert*-butylgallium (TTBGa) on the decomposition of *tert*-butylarsine (TBAs) and *tert*-butylphosphine (TBP) during growth of GaAs and GaP has been studied by mass spectrometry respectively. The decomposition of the precursors was investigated by a novel fast Fourier transform (FFT) quadrupole ion trap mass spectrometer (iTrap) inline in an MOVPE system.[2] The analyte is carried under stable flow and pressure conditions through a bypass system to achieve reliable and comparable measurement data. To overcome the large pressure difference between the reactor chamber (50 mbar) and the iTrap (ultrahigh vaccum - UHV) the analyte is then pulsed by an atomic layer deposition valve into the mass spectrometer. Due to the FFT base concept a single mass spectrum can be recorded in less than 2 s and with very high sensitivity (pptV).[3] This allows real time analysis of the gas phase reactions under realistic MOVPE conditions.

Results and Conclusions

Figure 1a) shows the recorded breakdown curves of TBAs on the bare susceptor and during GaAs growth with three different Ga precursors TMGa, TEGa and TTBGa. As comparison the measured breakdown curves of the individual Ga precursors are shown in figure 1b). From these curves the decomposition temperature (T_{decomp}) of the precursors can be determined with the temperature at which the detected intensities drop to half of their value. These values are listed in table 1.

TBAs	T_{decomp} = 360 ± 10 °C		
TBAs + TMGa	T_{decomp} = 300 ± 10 °C	TMGa	T_{decomp} = 340 ± 10 °C
TBAs + TEGa	T_{decomp} = 220 ± 10 °C	TEGa	T_{decomp} = 250 ± 10 °C
TBAs + TTBGa	T_{decomp} = 175 ± 10 °C	TTBGa	T_{decomp} = 140 ± 10 °C

Table 1: *Determined decomposition temperatures.*

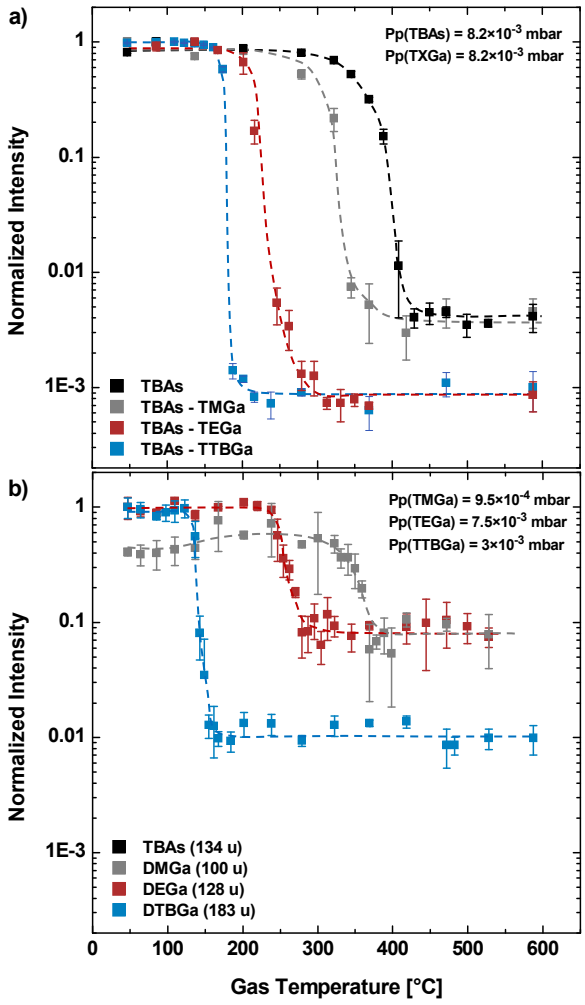

Figure 1: *a) Breakdown curves of TBAs on the bare susceptor and during GaAs growth with TMGa, TEGa and TTBGa. b) Breakdown curves of TMGa, TEGa and TTBGa on the bare susceptor.*

First of all, a clear trend for the unimolecular decomposition of the Ga precursors is visible. The decomposition temperature drops significantly with increasing size of the alkyl groups attached to the Ga. This fits to the common trend for metal-organic precursors.[4] As known from literature the TBAs decomposition should occur in the temperature range between TEGa and TMGa. This is not confirmed by our measurement. TBAs decomposes at slightly higher temperature compared to TMGa. On one hand the temperature determination is not that precisely and can vary between different measurement sessions due to the experimental setup. On the other hand, the different experimental parameters like reactor geometry, pressure, flow rate, partial pressures, carrier gas and the actual temperature can severely influence the decomposition. Nevertheless, a significant effect of the Ga precursors on the TBAs decomposition is observed. The bimolecular reactions lower the decomposition temperature of TBAs. These results and similar findings for GaP growth will be discussed in more detail in the presentation.

Outlook

Further gas phase investigations for GaAs and GaP growth will be performed, especially under different experimental settings since bimolecular reactions can strongly depend on the partial pressure of the supplied precursors. This hopefully gives more inside into the growth conditions used for meta stable alloys like mentioned above. Furthermore, novel precursors for growth of III/V semiconductors will be investigated.

References

[1] G. B. Stringfellow, J. Cryst. Growth 2004, 264 (4), 620−630.
[2] L. Nattermann, O. Maßmeyer, E. Sterzer, V. Derpmann, H. Y. Chung, W. Stolz, K. Volz, Sci. Rep. 2018, 8, 1.
[3] H. Y. Chung, M. Aliman, G. Fedosenko, A. Laue, R. Reuter, V. Derpmann, L. Gorkhover, M. Antoni 2016, 27th Annu. SEMI Adv. Semicond. Manuf. Conf. ASMC 2016, 263−266.
[4] G. B. Stringfellow, Organometallic Vapor-Phase Epitaxy: Theory and Practice. Academic Press (1990).

Investigation on Preparation of Interpnictogen Compounds for Possible Application in MOVPE

Christian Ritter, Carsten von Hänisch

Material Sciences Center and Faculty of Chemistry, Philipps-Universität Marburg

Introduction

Since the DTBAA precursor for growing dilute nitride GaAs semiconductors gained high attention due to significant better N incorporation than state of the art UDMHy the investigation of novel group 15 compounds for possible application in MOVPE come to the fore of interests.[1,2] Therefore especially interpnictogen molecules seems to provide a lot of unexploited potential. For a focused synthesis of novel precursors a fundamental investigation on the reactivity of this class of compounds is crucial. Up to now no molecule is known that contains all group 15 elements from nitrogen to bismuth. Beside the unknown quinternary only two quaternary interpnictogen compounds were prepared till now.[3,4]

Results

The conversion of $AsCl_3$ with an excess of *t*$BuNH_2$ leads to the *tert*-butyl amido substituted four membered nitrogen arsenic ring (*t*BuNH)$_2$(AsN*t*Bu)$_2$ (**1**) first described by Vetter *et al*. in 1964.[5] The lithiation and following conversion with $BiCl_3$ and $SbCl_3$ have been published, but only for the corresponding Sb compound sufficient analytical data were provided.[6,7] To this series I added the product of the conversion with $AsCl_3$. With the preparation of these compounds (**3**–**5**, Fig. 1) we obtained valuable synthons for further conversions with some binary interpnictogen compounds previously described within our group (*t*Bu_2As-P(Li)*t*Bu & *t*Bu_2Sb-P(Li)*t*Bu).[8]

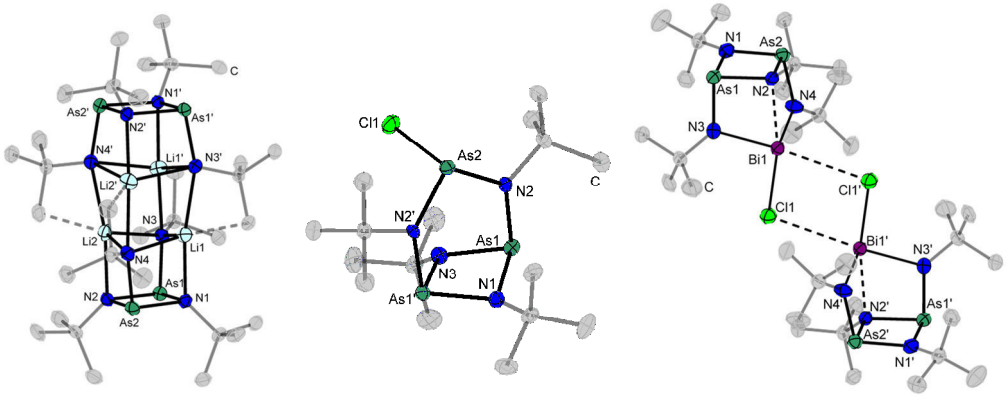

Figure 1: *Molecular structures of* ***2****,* ***3*** *and* ***5*** *in the solid state. Hydrogen atoms are omitted for clarity.*

Within the reaction of **3**–**5** with *t*Bu_2Sb-P(Li)*t*Bu the desired products were obtained and fully characterized (**6**–**8**, Fig. 2 top). **8** represents the first molecule containing all pnictogens atoms from nitrogen to bismuth. Furthermore it is surprisingly stable against room temperature and light, which is remarkable, since it contains a covalent bismuth phosphorus bond that is known to be very weak. The reason for this relative high stability is probably the chelating coordination from the two bonded nitrogen atoms as well as from one of the nitrogen atoms of the four membered ring with an additional weak interaction. In contrast, the reaction with *t*Bu_2As-P(Li)*t*Bu leads to reduction of **4** & **5** instead yielding the products **9** & **10** (Fig. 2 bottom).

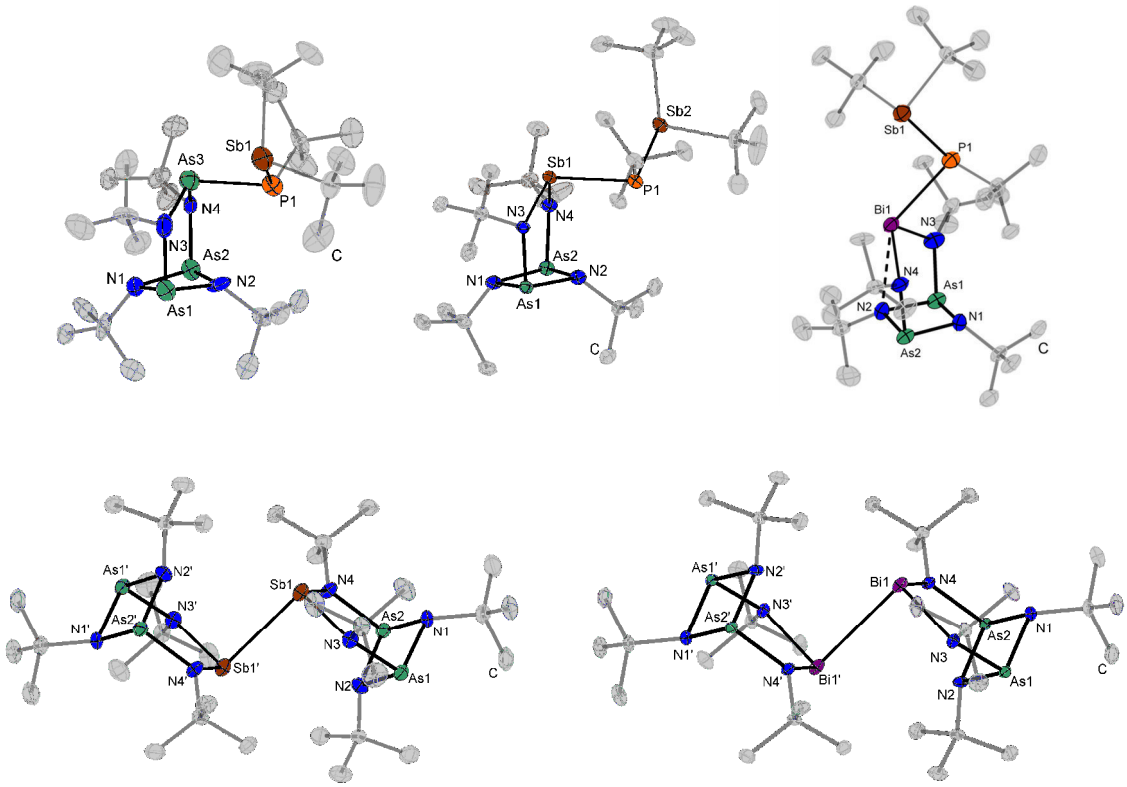

Figure 2: *Molecular structures of* ***6****–****8*** *(top) and* ***9*** *&* ***10*** *(bottom) in the solid state. Hydrogen atoms are omitted for clarity.*

Conclusion and Outlook

Motivated by the promising results of the DTBAA precursor in the MOVPE process we investigated the reactivity of compounds with elements of the group 15 mixed together. We did this to gain insights for future development of novel molecules with possible application as group 15 precursors. Therefore we synthesized two novel quaternary and the first quinternary interpnictogen compound containing all elements from nitrogen to bismuth. Future works will concentrate on preparing other element combinations and orders in this class of compounds. Based on those results we will synthesize novel interpnictogen precursors for future applications.

References

[1] E. Sterzer, A. Beyer, L. Duschek, L. Nattermann, B. Ringler, B. Leube, A. Stegmüller, R. Tonner, C. von Hänisch, W. Stolz, et al., *J. Cryst. Growth* **2016**, *439*, 19–27.

[2] E. Sterzer, B. Ringler, L. Nattermann, A. Beyer, C. von Hänisch, W. Stolz, K. Volz, *J. Cryst. Growth* **2017**, *467*, 132–136.

[3] R. Garbe, S. Wocadlo, H.-C. Kang, W. Massa, K. Harms, K. Dehnicke, *Chem. Ber.* **1996**, *129*, 109–113.

[4] A. Hinz, A. Schulz, A. Villinger, *Chem. Commun.* **2015**, *51*, 11437–11440.

[5] H.-J. Vetter, H. Nöth, W. Jahn, *Z. Anorg. Chemie* **1964**, *328*, 144–153.

[6] M. Veith, A. Rammo, M. Hans, *Phosphorus. Sulfur.* **1994**, *93*, 197–200.

[7] L. Belter, W. Frank, *Phosphorus Sulfur Relat. Elem.* **2016**, *191*, 675–677.

[8] B. Ringler, M. Müller, C. von Hänisch, *Eur. J. Inorg. Chem.* **2018**, *2018*, 640–646.

Further research summaries by GRK-members

(in alphabetical order)

Synthesis and Reactivity of Interpnictogen Compounds from Diaryl Halido Bismuthane

Tobias Dunaj, Carsten von Hänisch

Faculty of Chemistry and Material Sciences Center, Philipps-Universität Marburg

Introduction

Di-*tert*-butylarsane amine (DTBAA) can be used as precursor for the synthesis of 13/15-semiconductors via MOCVD methods. Using DTBAA and triethyl gallane, N-doped GaAs-semiconductors can be prepared. In comparison to the established procedure using *tert*-butyl arsane and 1,1-dimethyl hydrazine instead of DTBAA, a higher efficiency for nitrogen incorporation and a lower amount of carbon incorporation can be achieved.[1] In analogy to DTBAA, compounds with the formula $Aryl_2BiNH_2$ can be suitable as precursors for the preparation of bismuth and nitrogen doted semiconductors.

Only few compounds incorporating the structural motif $R_2Bi\text{-}PnR'_2$ (R = Alkyl-, Aryl-; R' = Alkyl-Aryl-, H; Pn = N-Sb) are described in the literature.[2-8] By reacting aryl substituted halido bismuthanes with metallated primary pnictogenides, we want to build binary interpnictogen compounds bearing functionalizable pnictogen substituents. These binary interpnictogen compounds are tested on their usability as precursors in MOCVD processes. Moreover, further functionalization to ternary and quaternary interpnictogen compounds is attempted.

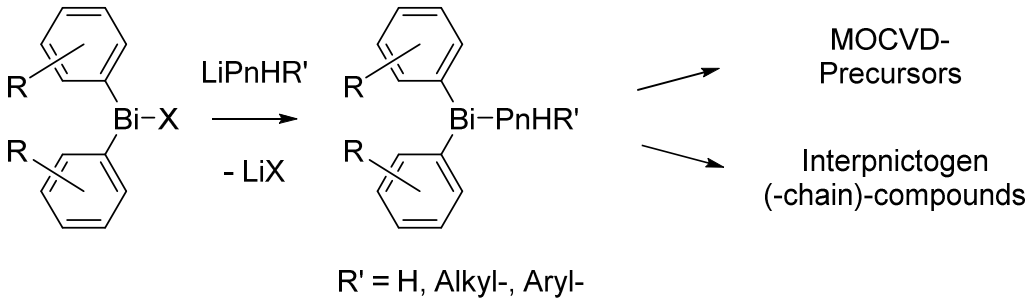

Scheme 1: *Aim of the study.*

Results

So far, three literature known diaryl halido bismuthanes (Ph_2BiCl,[9] Mes_2BiCl,[10] $Tripp_2BiCl$[11]) and the new Bis(2,6-diisoproylphenyl)bromobismuthane ($Dipp_2BiBr$) with varying steric bulk at the bismuth atom were prepared. First reactions indicate that the *tert*-butyl amine and *tert*-butyl phosphine substituted bismuthanes can be prepared by salt metathesis, though the corresponding binary interpnictogen compounds have not been isolated yet.

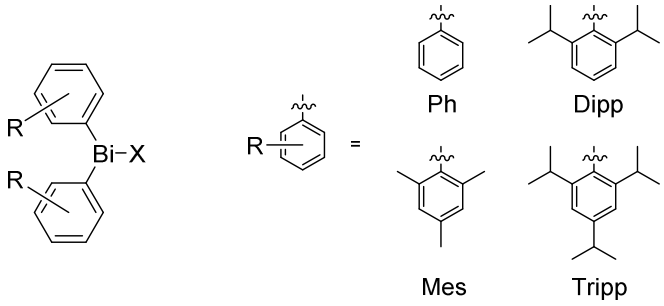

Scheme 2: *Used aryl substituents.*

Conclusion and Outlook

The performed reactions of the prepared diaryl halido bismuthanes with primary amides and phiosphides show promising results for the preparation of binary interpnictogen compounds. In future experiments the isolation of these compounds will be attempted. Moreover reactions with the lithiated compounds of the heavier primary pnictogenides will be executed. In analogy to DTBAA, preparation of compounds bearing a PnH_2-substituent will be achieved. The prepared binary interpnictogen compounds will be examined on their usability as MOCVD precursors and will be functionalized further to access ternary and quaternary interpnictogen compounds containing bismuth. Possible synthetic routes to achieve ternary and quaternary interpnictogen compounds are shown in scheme 3.

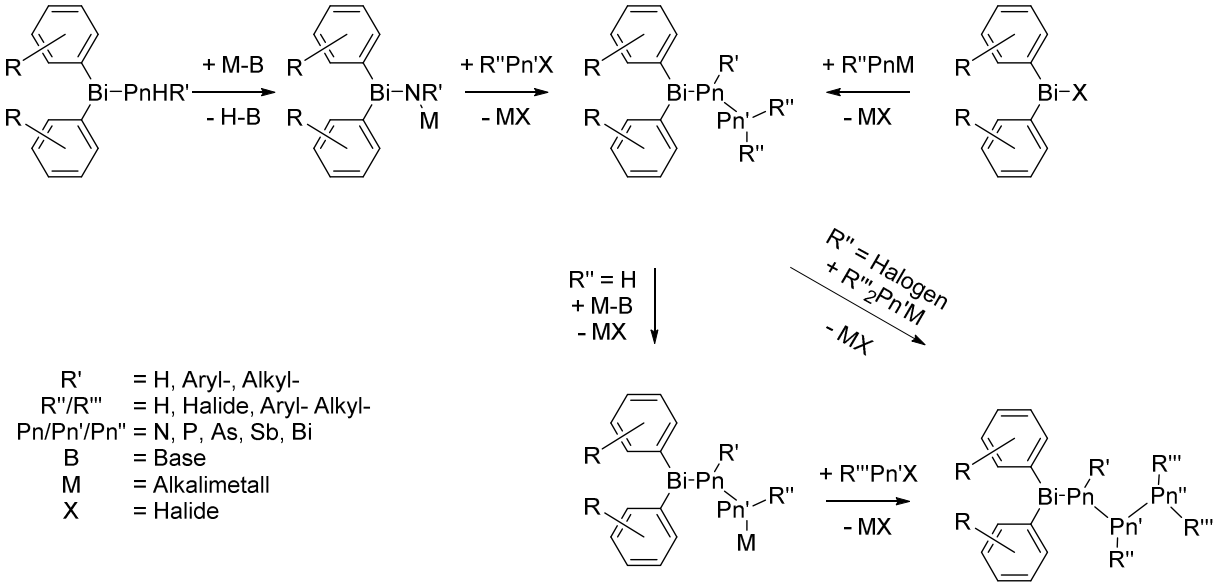

Scheme 3: *Possible reaction pathways to ternary and quaternary interpnictogen compounds from diaryl pnictogen bismuthanes.*

References

[1] C. von Hänisch, W. Stolz, K. Volz, *J. Cryst. Growth,* **2016**, *439*, 19-27

[2] O. J. Scherer, P. Hornig, M. Schmidt, *J. Organomet. Chem.,* **1966**, *3*, 259-264

[3] M. Nieger, G. Schafer, B. Ross, **CSD Commun.**, CCDC 233889, **2004**

[4] J. W. Wielandt, S. Petrie, N. L. Kilah, A. C. Willis, R. D. Dewhurst, F. Belaj, A. Orthaber, R. Stranger, S. B. Wild, *Aust J Chem*, **2016**, *69*, 524

[5] Y. Matano, H. Nomura, H. Suzuki, M. Shiro, H. Nakano, *J. Am. Chem. Soc.*, **2001**, *123*, 10954-10965

[6] C. Ritter, B. Ringler, F. Dankert, M. Conrad, F. Kraus, C. von Hänisch, *Dalton Trans.*, **2019**, *16*, 5253-5262

[7] A. J. Ashe III, E. G. Ludwig Jr., *J. Organomet. Chem.*, **1986**, *303 (2)*, 197-204

[8] H. J. Breunig, D. Müller, *Z. Naturforsch. B*, **1986**, *41B (9)*, 1129-1132

[9] D. H. R. Barton, N. Y. Bhatnagar, J. Flnet, W. B. Motherwell, *Tetrahedron.,* **1986**, *42 (12)*, 3111-3122

[10] X. W. Li, J. Lorberth, K. H. Ebert, W. Massa, S. Wocadlo, *J. Organomet. Chem.,* **1998**, *2*, 211- 215

[11] Y. Matano, M. Kinoshita, H. Suzuki, *Bull Chem. Soc. Jpn.,* **1992**, 3504-3506

Energy-filtered STEM – an experimental study using a fast, pixelated detector

S. Firoozabadi, D. Heimes, A. Beyer, K. Volz

Philipps-Universität Marburg, Physics, Marburg, Germany

Introduction

Scanning transmission electron microscopy (STEM) is widely applied for the characterization of nanostructures. The combination of high angle annular dark field (HAADF) images and image simulations considering only elastic scattering allowed quantitative evaluation on an atomic scale[1]. To this aim, multi-slice simulations based on the frozen lattice approximation are applied to compute the convergent beam electron diffraction (CBED) for every probe position and consequently the HAADF images[2]. There is a demand for measurements in the lower angular regime, for example when investigating light elements. However, there is a discrepancy between image simulations and measurements in the low-angle regime, which could be caused by neglecting the inelastic scattering in the simulations[3]. It is confirmed that incorporation of plasmon scattering improves the matching of simulated and experimental results for amorphous silicon[4]. In this study, considering the plasmon scattering via the STEMsalabim software package[2] the agreement between the simulated and the measured convergent beam electron diffraction (CBED) in low angular ranges is investigated.

As a simple model system for first investigations, silicon electron transparent samples are prepared in [010] direction by ion milling using a focused ion beam (JEOL JIB-4601F, JEOL Ltd.) and low voltage ion polishing using a NanoMill® (Model 1040, E. A. Fischione Instruments). The combination of a double aberration-corrected JEOL JEM2200FS operating at 200 keV (JEOL Ltd.) and an in-column, omega energy filter along with pre- and post-filter annular dark field (ADF) detectors allows atomic resolution energy filtered imaging[5]. Additionally, a pixelated detector (pnCCD (S)TEM Camera, PNDetector)[6] makes it possible to record the CBED at every probe position for unfiltered, zero-loss filtered, and plasmon-loss filtered conditions. Besides, taking into account inelastic scattering a modified version of the STEMsalabim software package is applied to simulate the CBED and STEM image intensities for an energy loss range of 0 to 40 eV[2,3].

Results

CBED patterns as well as position-averaged CBED (PACBED) patterns are recorded for the silicon specimen applying no energy filtering, zero-loss filtering and filtering at energetic positions where the plasmon peak arises. There are distinct differences in the angular dependence of the scattering/diffraction dependent on the energy range used. The Electron energy loss (EELS) spectrum of the silicon sample in [010] projection along with the ranges in which the energy is filtered is shown in Fig. 1a. The corresponding PACBEDs at each energy range are also illustrated in Fig. 1b. The intensity in all the images is normalized to the impinging beam so that a comparison with the image simulations is possible. The elastically scattered PACBED contains coherent information like thickness fringes more clearly than the unfiltered PACBED. In addition, Kikuchi lines in the PACBEDs show the existence of coherent scattering in case of inelastic as well as Plasmon peak filtered scattering. The unfiltered synthetic image integrated from the CBEDs recorded with the pixelated detector for an angular range of 30 – 60 mrad is shown as an inset of the unfiltered PACBED.

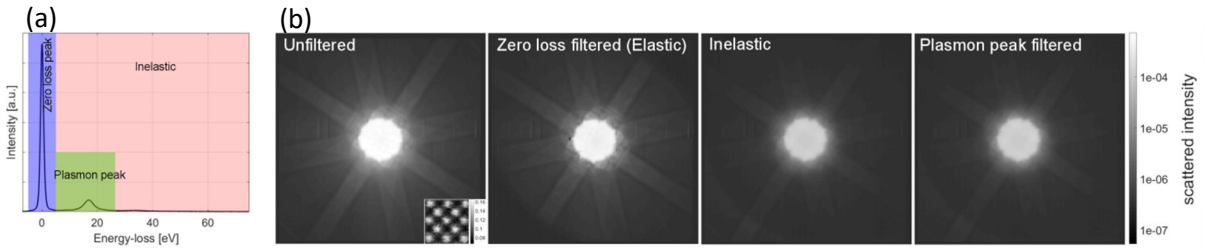

Figure 1: *(a) EELS spectrum of silicon [010] measurement along with the position of the energy slit for the PACBED measurement. (b) Corresponding PACBEDs at each energy range illustrated on the EELS spectrum.*

The azimuthally integrated intensity for different angles calculated from unfiltered, elastic, and inelastic PACBEDs (Fig. 1a) can be seen in Fig. 2a. In addition, Fig. 2b shows the ratio of inelastic to elastic scattering for different angles. The ratio is almost constant except for the angular range of around 14 – 35 mrad. It defines the angular dependency of plasmon scattering with respect to the elastic scattering.

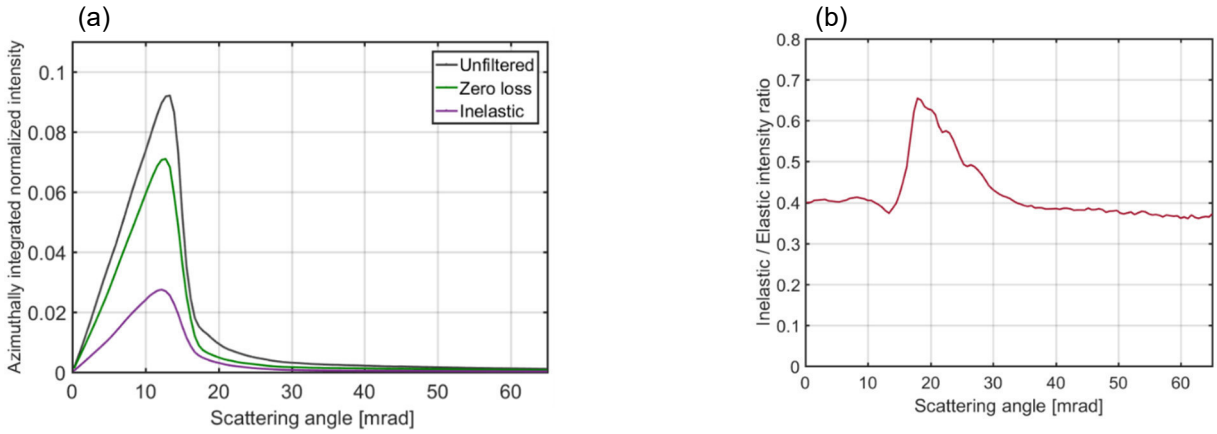

Figure 2: *(a) Azimuthally integrated scattered intensity for different angles calculated from unfiltered, elastic, and inelastic PACBEDs. (b) The ratio of inelastic to elastic scattering for different angles.*

Conclusion

In this work, unfiltered, inelastic, plasmon-loss as well as zero-loss filtered STEM diffraction patterns are investigated with the example of single crystalline silicon using a fast, pixelated detector. The results highlight features related to inelastic scattering in the angular range below 35 mrad.

Outlook

It is found that the specimen thickness is a crucial parameter to match experiment and simulation quantitatively. As the inelastic scattering is correlated to the plasmon mean-free-path (λ), a more accurate determination of λ can improve the agreement between the simulation and experiment. Hence, we determine the sample's thickness using different methods and calculate λ to apply it for the simulations. After determination of λ, the role of inelastic scattering becomes clear by comparing CBEDs after energy-filtering in the elastic and inelastic region of the spectrum. The same investigation can be applied on different single crystalline materials (e. g. Pt), binary materials (e. g. GaP) and ternary materials (e. g. GaNAs). Better matching of simulation and experiments for low angles can enable the quantitative evaluation of materials containing light elements (e. g. GaNAs).

References

[1] LeBeau, J. M., et al. "Quantitative atomic resolution scanning transmission electron microscopy." Physical Review Letters 100.20 (2008): 206101.

[2] Oelerich, J. O., et al. "STEMsalabim: A high-performance computing cluster friendly code for scanning transmission electron microscopy image simulations of thin specimens." Ultramicroscopy 177 (2017): 91-96.

[3] Müller-Caspary, K., et al. "Materials characterisation by angle-resolved scanning transmission electron microscopy." Scientific reports 6 (2016): 37146.

[4] Mkhoyan, K. A., et al. "Critical role of inelastic interactions in quantitative electron microscopy." Physical review letters 100.2 (2008): 025503.

[5] Hutchison, J. L., et al. "A versatile double aberration-corrected, energy filtered HREM/STEM for materials science." Ultramicroscopy 103.1 (2005): 7-15.

[6] Ryll, H., et al. "A pnCCD-based, fast direct single electron imaging camera for TEM and STEM." Journal of Instrumentation 11.04 (2016): P04006.

Adsorption of diphenols on Si(001) studied by means of XPS

Timo Glaser, Julian Heep, Christian Länger, and Michael Dürr

Institut für Angewandte Physik, Justus-Liebig-Universität Gießen, D-35392 Gießen

Introduction

On semiconductor surfaces, organic molecules typically adsorb via an intermediate state; if a heteroatom is involved, this intermediate often involves a dative bond[1]. Alcohols, for example, adsorb on Si(001) via an intermediate state comprising a dative bond between the oxygen atom of the OH-group and the lower silicon atom of the silicon dimer with its unfilled dangling bond[2,3]. Diphenols contain two OH-groups; there are three different diphenols which differ in the position of the two OH-groups with respect to each other. Diphenols are thus an ideal test system to investigate the influence of the structure of bifunctional molecules on their adsorption behavior. Indeed, for Ge(001), the adsorption of diphenols has already been investigated; dependent on the relative position of the OH-groups in the molecule and surface coverage, different ratios of single and double bound diphenols have been observed[4].

Results

We investigated the adsorption of diphenols on Si(001) at room temperature by means of X-ray photoelectron spectroscopy (XPS). In agreement with earlier results on the adsorption of alcohols[3], the C 1s and O 1s spectra indicate covalent adsorption via the oxygen atom which goes along with O-H cleavage and a covalent bonding of the H atom on the silicon surface. For all diphenols, a single-binding and a dual-binding configuration on Si(001) was observed. For hydroquinone with the OH-groups arranged in para-position, the coverage saturates at 0.5 ML (1 ML equals one molecule per dimer); at low coverage, the dual-binding configuration is dominant (80 %). With increasing coverage, the percentage of the single-binding configuration slightly increases up to 30 %. For resorcinol, with the OH-groups being arranged in meta-position, the coverage saturates at 0.6 ML. At low coverage, the dual-binding configuration is again dominant (75 %). With increasing coverage, the percentage of the single-binding configuration is increasing up to a maximum of 45 %. For catechol, with the OH-groups arranged in ortho-position, the coverage also saturates at 0.6 ML. At low coverages it shows a similar adsorption behavior as hydroquinone and resorcinol.

Conclusion & research plan

The results demonstrate how the detailed structure of bifunctional molecules can influence their adsorption behavior. In order to directly monitor the adsorption kinetics of the different diphenols, in-situ XPS measurements will be carried out at a synchrotron X-ray source. Varying the surface temperature and flux of the incoming molecules will then give further insight in how to control the adsorption of bifunctional molecules on silicon.

References

[1] Y. H. Min, H. Lee, D. H. Kim, and S. Kim, Dative Bonding of Organic Molecules in “Functionalization of Semiconductor Surfaces”, pp 193, Wiley (2012).
[2] T. Kato, S. Y. Kang, X. Xu, and T. Yamabe, J. Phys. Chem. B 105, 10340 (2001).
[3] C. Länger, T. Bohamud, J. Heep, T. Glaser, M. Reutzel, U. Höfer and M. Dürr, J. Phys. Chem. C 122, 14756 (2018).
[4] B. Shong, R. Y. Brogaard, T. E. Sandoval and S. F. Bent, J. Phys. Chem. C 118, 23811 (2014).

MOVPE Growth and Characterization of GaAs based W Type Ga(N,As)/Ga(As,Bi)/Ga(N,As) Quantum Well Heterostructures

R. Günkel, T. Hepp, K. Volz

Wissenschaftliches Zentrum für Materialwissenschaften und Fachbereich Physik, Philipps-Universität Marburg

Introduction

Due to the demand for fiber optic networks, the energy consumption of the Internet continues to rise[1]. An increasing amount of the energy is consumed by telecom lasers[2]. To significantly increase in efficiency it would be desirable to suppress the Auger transitions as main loss mechanism. One possibility to achiev this situation is to exploit type-II transition for laser application[3],[4]. The relevant transition takes place over the interfaces of adjacent quantum wells (QWs). In this case, the electron states are located in Ga(N,As) QW and the hole states in the Ga(As,Bi) QW. By adjusting the composition and thickness of these adjacent quantum wells, it is possible to tune the transition energy. In order to increase the transition probability for a type-II transition, it is appropriate to use a so-called W Type structure (see Fig. 1).

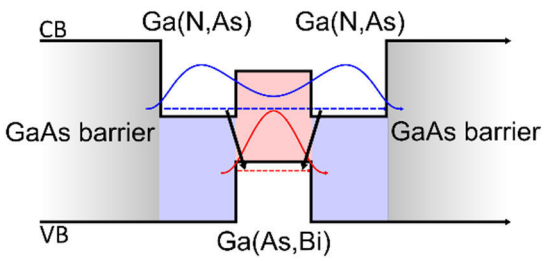

Figure 1: *Schematic illustration of W Type quantum well heterostructure consisting of a Ga(As,Bi) hole QW embedded in between two Ga(N,As) electron QWs. The energetic position of the electron and the hole ground states are illustrated as dashed blue or red lines. Furthermore, the respective wave functions are illustrated as blue or red lines. Possible type-II transitions are indicated as black arrows.*

Results

The Ga(N,As) and the Ga(As,Bi) triple quantum wells (3QW) were grown by metal organic vapor phase epitaxy (MOVPE). After the characterization and the quality testing of these test structures, W Type structures were grown while the QWs were grown under the same growth conditions as the single Ga(N,As) or Ga(As,Bi) QWs, respectively.The high resolution X-ray diffraction (HR-XRD), photoluminescence (PL) and atomic force microscope (AFM) measurements showed that high quality samples were obtained.

RTA was carried out to check for further improvement of the optical quality, which is often observed in dilute N containing materials. Fig. 2 shows the improvement factor of the temperature dependent annealing series for Ga(N,As) 3QW test structure. As expected, the intensity improvement factor first increases to a maximum and then decreases again. The peak of this series can be determined at 650 °C for 10 s. In addition, Fig. 2 shows the FWHM values of the measurement series. However, no trend and only maximum difference of 4 meV can be identified by analysing these FWHM values.

Detailed improvements of the W Type structure concerning the growth conditions including the optimisation of the single Ga(N,As) and Ga(As,Bi) QWs will be presented on the poster.

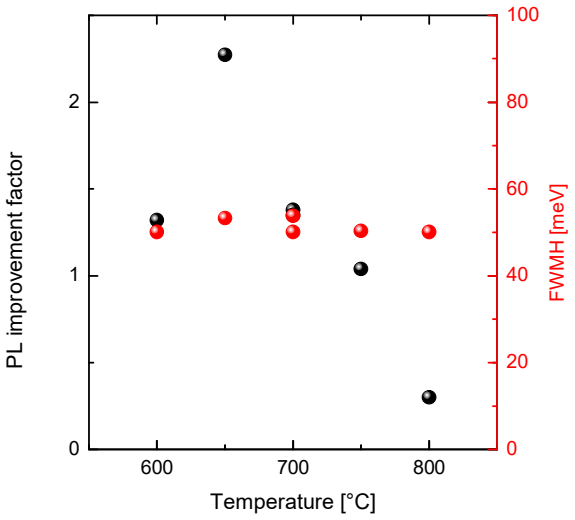

Figure 2: *Plot of PL intensity improvement factor and FWHM values against the annealing temperature. The Ga(N,As) samples were annealed for 10 s each at the appropriate temperature using the RTA.*

Outlook

An important step is the integration of this W Type structure as an active region into a typical laser architecture on GaAs. First, such a laser will be grown by MOVPE and characterized. In subsequent growth series the emission wavelength will be shifted by optimizing the sample structure (e. g. thickness, composition) for telecom applications.

References

[1] Rodney S. Tucker et al., "Energy consumption in IP networks", *34th European Conference on Optical Communication*. IEEE, 2008.

[2] S. J. Sweeney, A. F. Phillips, A. R. Adams, E. P. O'Reilly, and P. J. A. Thijs, "The effect of temperature dependent processes on the performance of 1.5-*μ*m compressively strained InGaAs(P) MQW semiconductor diode lasers", *IEEE Photonics Technology Letters*, 10(8):1076–1078, 1998.

[3] C. A. Broderick et al., "$GaAs_{1-x}Bi_x/GaN_yAs_{1-y}$ type-II quantum wells: novel strain-balanced heterostructures for GaAs-based near- and mid-infrared photonics", *Sci. Rep.* 7 (2017) 46371

[4] Christian Fuchs, "Epitaxial growth and characterization of GaAs-based type-II (GaIn)As/Ga(AsSb)/(GaIn)As "W"-quantum well heterostructures and lasers." *PhD thesis*, Philipps-Universität Marburg, 2017.

ORGANO-FUNCTIONALIZED TETREL CHALCOGENIDE CLUSTERS

Katharina Hanau, Stefanie Dehnen

Faculty of Chemistry and Material Sciences Center, Philipps-Universität Marburg

Introduction

Preliminary work in our group has shown that the structure of tetrel sulfide clusters (heteroadmantane vs. double-decker vs. defect heterocubane vs. bis-defect-heterocubane) and their properties are influenced by the choice of the elements, as well as the organic moiety.[1,2] The adamantane-type cluster $[(StySn)_4S_6]$ is of special interest, as it shows extreme nonlinear optical properties and acts as a highly directional white-light emitter upon irradiation by a continuous-wave laser diode.[3] Furthermore, the organic moieties and the cluster core can be modified in subsequent reactions. An example is the formation of a rugby-ball-like molecule derived from reactions of the double-decker-type cluster $[(R^1Sn)_4S_6]$ ($R^1 = CMe_2CH_2COMe$) with bifunctional spacers $H_2N\text{-}X\text{-}NH_2$ ($X = (NH)_2CO$, $(NH)_2C_{10}H_6$).[4]

Results

The reactions of $[(R^1Sn)'_3Se4]$ ($R^1 = CMe_2CH_2C(O)Me$) with different dihydrazides or dihydrazines yield new capsule-like compounds of the type $[(\mu\text{-}R)_3(Sn_3Se_4)_2][X]_2$ ($R = (CMe_2CH_2C(Me)NNHC(O))_2(CH_2)_4$, $(CMe_2CH_2C(Me)NNH)_2C_{10}H_6$, $X = Cl$, $SnCl_3$).[5] As shown in Fig. 1, these capsules differ in their inner volumes and the molecules incorporated within depend on the organic moiety used.

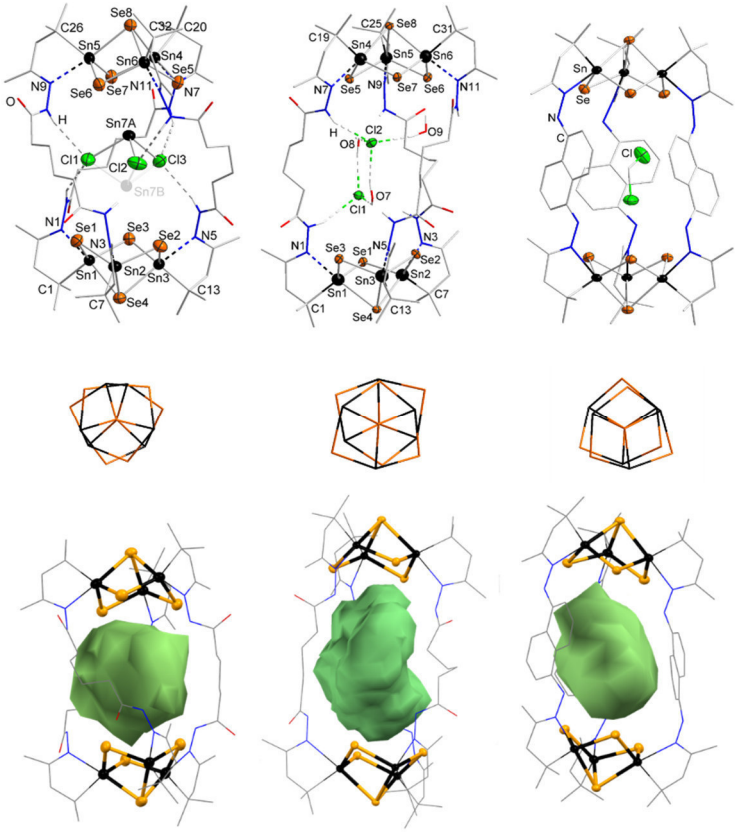

Figure 1: *Molecular structures of the capsule-type clusters $[(\mu\text{-}R)_3(Sn_3Se_4)_2][X]_2$ (top) and their defect-heterocubane units' relative orientation (center). The bottom picture shows the visualization of the inner volumes (from left to right): 145.5 Å³, 162.0 Å³, and 134.0 Å³. H atoms and anions not incorporated within the capsules are omitted for clarity.*

Whereas the flexibility of the adipinic acid hydrazide ligands allows for two different capsules with different orientations of the defect-heterocubane units to each other as well as different

inner volumes and anions, there is only one capsule-type with the naphthyl hydrazine ligand. A comparison with the analogous tin sulfide cluster shows an only slightly smaller inner volume in that cluster, indicating that the organic ligand has the biggest impact in that regard.

The reaction of organotrichloro silanes $RSiCl_3$ with Na_2S yields the adamantane-type clusters $[(RSi)_4S_6]$ (R = Ph, Naph). These were analyzed via single-crystal X-ray diffraction, NMR spectroscopy and mass spectrometry. Investigating the clusters' reactivity towards transition metal complexes led to fragmentation reactions under formation of $[Ph_3PAuS(R)SiS]_2$. Fig. 2 shows the reaction pathway using the example of the naphthyl-derivative. As of yet, the existence of the analogous styryl-substituted clusters could only be verified via ^{29}Si NMR spectroscopy, which showed the formation of one new silicon species with a downfield shift of approx. 10 ppm in regard to the starting compound. This is in accordance with the formation of an adamantane-type silicon sulfide cluster, as reported in the literature.[6]

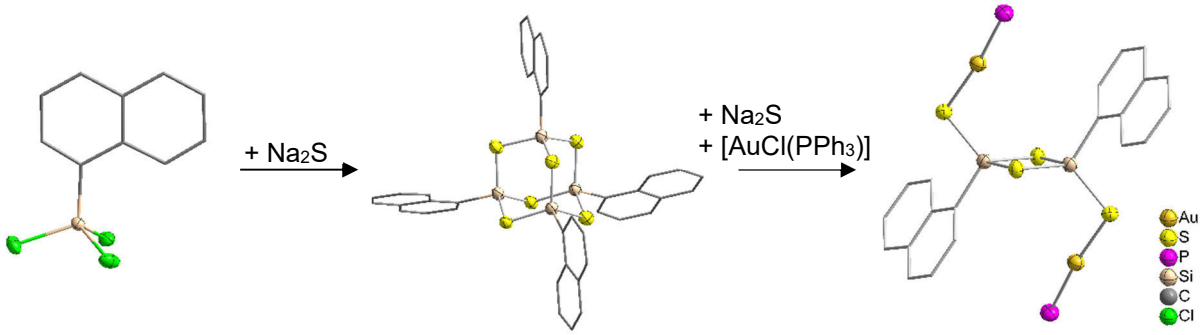

Figure 2: *Synthesis of organo-functionalized silicon sulfide clusters (phenyl groups and H atoms omitted for clarity).*

Conclusions

Several new tetrel chalcogenide clusters were obtained by reacting chalcogenide sources, such as $(SiMe_3)_2Se$ or Na_2S, with the correspondent tetrel compound. Rugby-ball-like molecules were synthesized by reacting the defect heterocubane-type cluster $[(R^1Sn)_3Se_4]$ with bifunctional spacers of the general type $H_2N\text{-}X\text{-}NH_2$ (X = alkyl chain, (hetero)cycle). Reacting organotrichloro silanes with Na_2S yields adamantane-type clusters, which undergo follow-up reactions with $[AuCl(PPh_3)]$ and Na_2S to form Si_2S_2 four-membered rings with linear $SAuPPh_3$ substituents.

Outlook

Currently, the reactivity of $[(StySi)_4S_6]$ towards $[AuCl(PPh_3)]$ is investigated in order to isolate an analogue to the known compounds based on four-membered Si_2S_2 rings, and thus to find further proof for the existence of yet elusive $[(StyS)_4S_6]$. In future work, the optical properties of these new silicon sulfide compounds are to be investigated and compared to those of the analogous tin sulfide clusters.

References

[1] Z. Hassanzadeh Fard, L. Xiong, C. Müller, M. Holynska, S. Dehnen, *Chem. Eur. J.* **2009**, *15*, 6595 – 6604.

[2] J. P. Eußner, B. E. K. Barth, E. Leusmann, Z. You, N. Rinn, S. Dehnen, *Chem. Eur. J.* **2013**, *19*, 13792 – 13802.

[3] N. W. Rosemann, J. P. Eußner, A. Beyer, S. W. Koch, K. Volz, S. Dehnen, S. Chatterjee, *Science* **2016**, *352*, 1301–1304.

[4] Z. Hassanzadeh Fard, M. R. Halvagar, S. Dehnen, *J. Am. Chem. Soc.* **2010**, *132*, 2848 – 2849.

[5] K. Hanau, N. Rinn, M. Argentari, S. Dehnen, *Chem. Eur. J.* **2018**, *24*, 11711 – 11716.

[6] H.-G. Horn, M. Hemeke, *Chemiker-Ztg.* **1982**, *106*, 263 – 266.

Adsorption of benzylazide on Si(001) – a combined STM and XPS investigation

Julian Heep[1], Christian Länger[1], Jannick Meinecke[2], Ulrich Koert[2], and Michael Dürr[1]

[1]Institut für Angewandte Physik, Justus-Liebig-Universität Gießen, D-35392 Gießen
[2]Fachbereich Chemie, Philipps-Universität Marburg, D-35032 Marburg

Introduction

The adsorption of organic molecules on silicon surfaces is intensively investigated. In part, this is due to possible future applications of such hybrid systems, including, among others, microelectronic devices (“more than Moore”). In the context of such organic functionalization, azides may play an important role[1]. In this work, the reaction of benzylazide on Si(001) was investigated by means of STM and XPS. In literature, it is indicated that benzylazide reacts via N_2-elimination into one final state on Si(001)[2,3]. In this state, the remaining nitrogen is bonded with both silicon atoms of a dimer, the aromatic ring of benzylazide stays intact.

Results

Our XPS studies for various sub-monolayer coverages up to saturation coverage indeed show clear evidence for a reaction via N_2-elimination at room temperature and 150 K. After adsorption, the benzylazide consisting of 8 carbon- and 3 nitrogen-atoms yields a signal ratio of the C 1s and N 1s signals of 8 to 1 (cross-section corrected) on the silicon surface, indicating the loss of two nitrogen atoms per molecule.

STM images at room temperature on the other hand show that the system is by far more complicated than the XPS analysis might suggest. Images taken at positive sample bias clearly show two different features, a dark one and a bright one, with comparable abundance. All features observed in negative sample bias images are bright, but two different configurations can be distinguished as well. When quantitatively analyzing the height profiles, a clearly bimodal distribution was observed. In contrast, STM images taken at 50 K (adsorption temperature: 50 K, positive sample bias) only show one type of bright features, which is different with respect to all features observed at room temperature at the same sample bias.

Conclusion

It was clearly shown that benzylazide reacts on Si(001) into two distinct final states. The reaction pathway proceeds for both configurations via N_2-elimination including an intermediate state, which was isolated and observed by means of STM at 50 K.

Outlook

In the future, the exact configurations will be investigated in collaboration with theory. Further reaction pathways and ways of controlling this reaction will be addressed, among others by short heating pulses induced by ns-laser-heating of the sample.

References

[1] N. Münster, P. Nikodemiak, and U. Koert, Org. Lett. **18**, 4296 (2016).
[2] S. Bocharov, O. Dmitrenko, L. P. Méndez De Leo, and A. V. Teplyakov, J. Am. Chem. Soc. **128**, 9300 (2006).
[3] T. R. Leftwich and A. V. Teplyakov, J. Phys. Chem. C **112**, 4297 (2008).

Improved Frozen Lattice Approximation by First Principles Phonon Calculations

D. Heimes*, S. Firoozabadi, A. Beyer, J. O. Oelerich, K. Volz

Faculty of Physics and Material Sciences Center, Philipps-Universität Marburg
**damien.heimes@physik.uni-marburg.de*

Introduction

Scanning transmission electron microscopy (STEM) is a method, which achieves resolutions in the sub angstrom range. This makes it possible to image single atomic columns. In order to gain quantitative data from experiments, the comparison to accurate simulations is necessary. Effects that have a great influence on experimentally gained images also have to be taken into account in simulations. One of those is thermal diffuse scattering (TDS), which is caused by the oscillations of atoms due to their temperature. Fig. 1 shows that TDS leads to a redistribution of the image intensity from the atomic columns to the background.

In most cases TDS is simulated by displacing the atoms randomly from their equilibrium positions. This suffices in many cases, but there are certain features in convergent beam electron diffraction patterns (CBEDs), which cannot be reproduced by this. In order to do so, one has to incorporate correlated atomic movement.

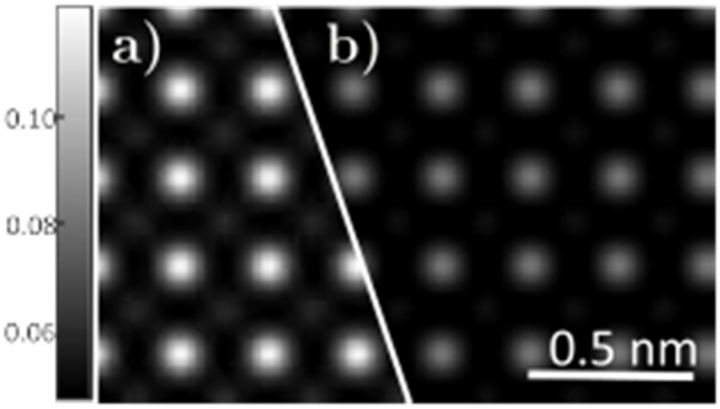

Figure 1: *Simulated gallium phosphide STEM images, at 0 K (a) and 300 K (b). Taken from [2]*

Results and conclusions

A code was written to implement a method to produce atomic displacements, which include correlated atomic movement[1]. This method uses phonon frequencies and eigenvectors, which have been calculated by density functional theory (DFT).

The code was applied for Si [001] in order to reproduce results from [1] as a proof of principle. Atomic displacements from this code were used to carry out STEM image simulations with the STEMsalabim code[2]. The resulting CBEDs show features, which can only be reproduced by applying correlated atomic movement[1], see Figure 2. This proves that the generated displacements do reproduce the expected results and that correlated atomic movement plays a significant role at low scattering angles.

Outlook

The mean squared displacement (MSD) depends on the set of points in reciprocal space, at which the phonons are calculated. There are still deviations from the literature values for the MSD. The right choice for the set of points will be subject of further investigations. After that, the next step will be to verify that the method also gives accurate results for other materials.

The method shall be made usable for STEMsalabim users. More importantly, the method can also be applied to calculate the MSD for materials with so far unknown MSD.

Future work will also include convergence analysis of STEM simulations with respect to the number of phonon configurations and the implementation of further effects to the STEMsalabim code, like e. g. going beyond the isolated atoms approach in order to include effects caused by atomic bonds.

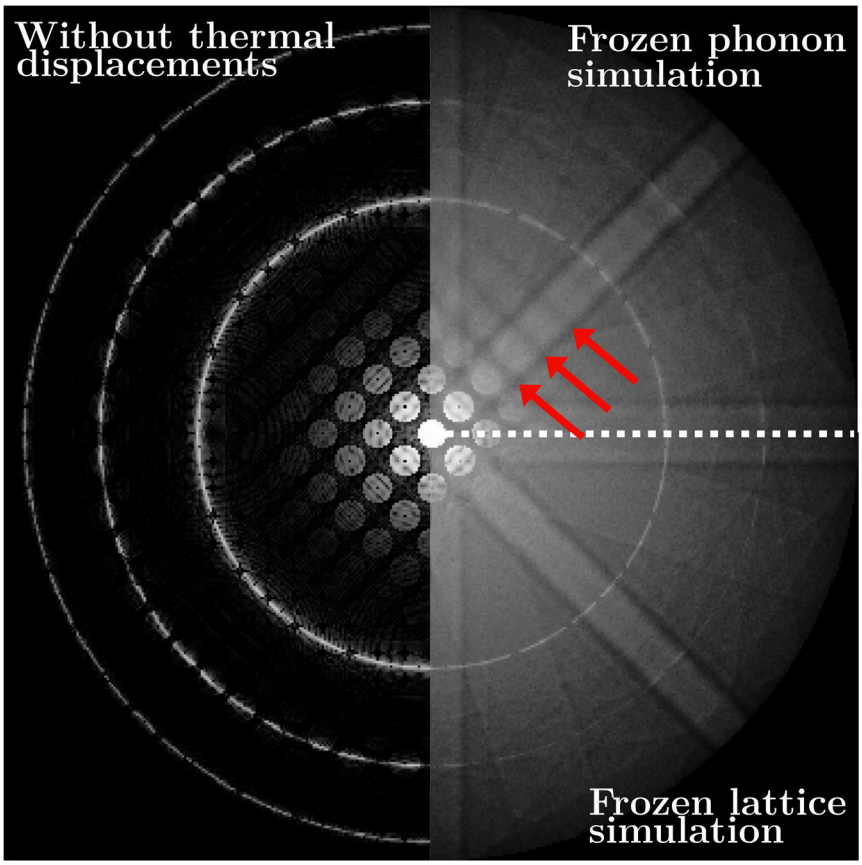

Figure 2: *CBED pattern for Si in [001] direction for different sets of atomic displacements. The left half shows the case for zero displacements, i. e. T = 0 K. The upper right quarter shows the result for displacements generated with the correlated FP method, the lower right quarter for displacements from uncorrelated random displacements. The features that are only reproducible by correlated atomic movement are indicated by red arrows. The result is in very good agreement with [1].*

References

[1] D. A. Muller et al. ‘Simulation of thermal diffuse scattering including a detailed phonon dispersion curve.’ Ultramicroscopy 86, 3-4: 371 (2001)

[2] J. O. Oelerich et al. ‘STEMsalabim: A high-performance computing cluster friendly code for scanning transmission electron microscopy image simulations of thin specimens.’ Ultramicroscopy 177: 91 (2017)

Sila crown ethers and their coordination towards *p*-block cations

Marcel Köster, Carsten von Hänisch

Faculty of Chemistry and Material Sciences Center, Philipps-Universität Marburg

Introduction

Organic ethers and especially the cyclic crown ethers, discovered by *Charles Pedersen* 1967, have found wide applications as chelate ligands.[1-4] However the silyl ethers do not show a similar complexation capability due to a lesser basicity of the oxygen atom in the Si-O bond and only few complexes with cyclic silyl ethers as D_6 or D_7 (D = -$SiMe_2O$-) can be found in the literature.[5-8] A possible explanation for this behavior is the electrostatic repulsion between the positively polarized silicon atom in the Si-O bond and the cation to coordinate.[9,10] Another explanation implies a negative hyperconjugation of an occupied *p*-orbital of the oxygen atom into a σ*-orbital of the Si-R bonds (R = H,C). This would weaken the Si-R-bonds as well as strengthen the Si-O bonds and thus leading to a lesser basicity of the oxygen atom.[11,12] To reduce the positive polarization of the silicon atoms we insert disilane units in our working group forming hybrid crown ethers (s. scheme 1).[13] With these disila and tetrasila crown ethers it is possible to coordinate alkaline metal and earth alkaline metal cations.[13-15] In this work we intended to transfer this coordination chemistry to *p*-Block cations.

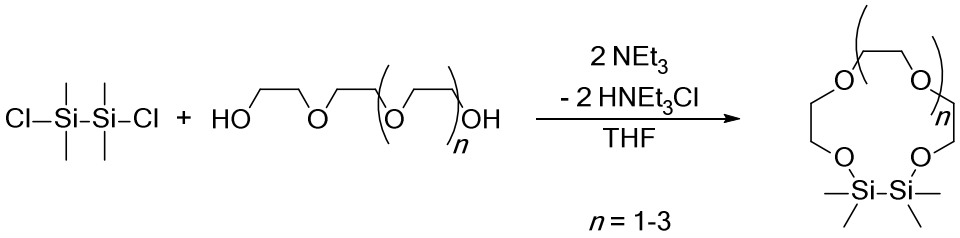

Scheme 1: *Synthesis of disilacrown ethers.*

Results

We focused on using low valent metal cations to examine the behavior of the non-bonded electron pairs at the *p*-block element in the possible complexes. According to this we investigated the reaction of InCl and TlCl with different hybrid crown ethers. This led to the formation of the complexes [In(1,2-disila[15]crown-5)][$GaCl_4$] (**1**) and [Tl(1,2-disila[18]crown-6)][$GaCl_4$] (**2**) which could be characterized by ^{1}H-, ^{13}C- and ^{29}Si-NMR- and IR-spectroscopy, crystal structure- and elemental analysis as well as HOMO-LUMO calculations.

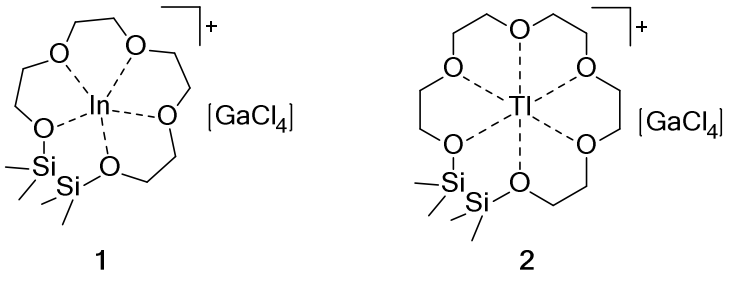

Figure 1: *Disila crown ether complexes **1** and **2** with group 13 cations.*

A similar reaction with the group 14 salts $GeCl_2$·dioxane, $SnCl_2$ and $PbBr_2$ resulted in receipt of colourless oils. Thus we modified the reaction by forming *in situ* the triflate anion containing derivates $Ge(OTf)_2$, $Sn(OTf)_2$ and $Pb(OTf)_2$ using trimethylsilyl trifluoromethanesulfonate. A coordination of these salts with 1,2-disila[15]Krone-5 led to the complexes [OTfM(1,2-disila[15]crown-5)][OTf] (M = Ge **3**, Sn **4**, Pb **5**). With the tetrasila crown ether 1,2,4,5-tetrasila-

benzo[15]crown-5, which can be synthesized in a similar reaction as the other hybrid crown ethers[16], we were able to receive a siloxane coordination to a *p*-block cation. The compound in [SnCl(1,2,4,5-tetrasila-benzo[15]krone-5)]$_2$[Sn(OTf)$_4$] (**6**) was obtained by the reaction with $SnCl_2$ as educt. All the complexes are characterized by ^{1}H-, ^{13}C- and ^{29}Si-NMR- and IR-spectroscopy, crystal structure- and elemental analysis.

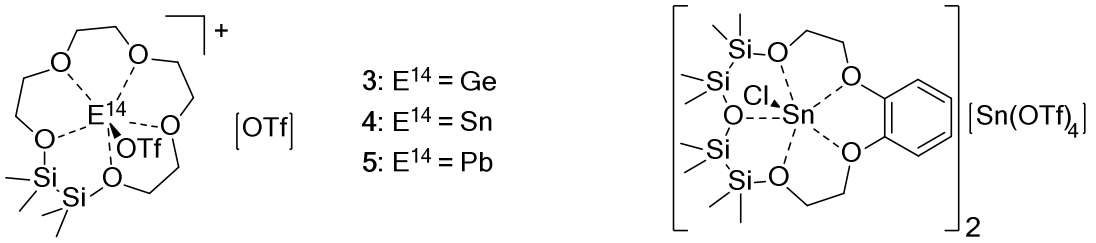

3-5 6

Figure 2: *Disila crown ether complexes **3-5** with group 14 cations and the tetrasila crown ether complex **6**.*

With $SbCl_3$ and $BiCl_3$ we were able to synthesize the group 15 complexes [TfOSbCl(1,2-disila[15]crown-5)][OTf] (**7**) and [TfOBiCl(1,2-disila[15]crown-5)][OTf] (**8**) in an analogue manner.

Conclusion and Outlook

We showed that the disila and tetrasila crown ethers are able to form complexes with diverse *p*-block cations. In the upcoming works we will increase the amount of the disila units in the hybrid crown ethers for further coordination chemistry. To complete the series of the group 13 cations we intend to coordinate our sila crown ethers with different gallium salts. Furthermore we plan to incorporate normal valent metal salts as $GaCl_3$ or $InCl_3$ in the hybrid ethers and to compare these complexes with the In^+ and Tl^+ compounds mentioned above.

References

[1] C. J. Pedersen, *J. Am. Chem. Soc.* **1967**, *89*, 7017–7036.
[2] J. J. Christensen, D. J. Eatough, R. M. Izatt, *Chem. Rev.* **1974**, *74*, 351–384.
[3] J. W. Steed, Coord. *Chem. Rev.* **2001**, *215*, 171–221.
[4] G. W. Gokel, W. M. Leevy, M. E. Weber, *Chem. Rev.* **2004**, *104*, 2723–2750.
[5] A. Decken, J. Passmore, X. Wang, *Angew. Chemie Int. Ed.* **2006**, *45*, 2773–2777.
[6] A. Decken, A. Leblanc, J. Passmore, X. Wang, *Eur. J. Inorg. Chem.* **2006**, 4033–4036.
[7] R. D. Ernst, A. Glöckner, A. M. Arif, *Z. Krist.* **2007**, *222*, 333–334.
[8] T. S. Cameron, A. Decken, I. Krossing, J. Passmore, J. M. Rautiainen, X. Wang, X. Zeng, *Inorg. Chem.* **2013**, *52*, 3113–3126.
[9] T. Kudo, S. Nagase, *J. Am. Chem. Soc.* **1985**, *107*, 2589–2595.
[10] M. S. Gordon, T. J. Packwood, M. T. Carroll, *J. Phys. Chem.* **1991**, *95*, 4332–4337.
[11] S. Shambayati, J. F. Blake, S. G. Wierschke, W. L. Jorgensen, S. L. Schreiber, *J. Am. Chem. Soc.* **1990**, *112*, 697–703.
[12] F. Weinhold, R. West, *Organometallics* **2011**, *30*, 5815–5824.
[13] K. Reuter, M. R. Buchner, G. Thiele, C. von Hänisch, *Inorg. Chem.* **2016**, *55*, 4441–4447.
[14] F. Dankert, K. Reuter, C. Donsbach, C. von Hänisch, *Dalt. Trans.* **2017**, *46*, 8727–8735.
[15] K. Reuter, G. Thiele, T. Hafner, F. Uhlig, C. von Hänisch, *Chem. Commun.* **2016**, *52*, 13265–13268.
[16] F. Dankert, C. von Hänisch, *Inorg. Chem.* **2019**, *58*, 3518–3526.

Ab-initio based calculation of the optical and electronic properties of dilute Ga(SbBi)

Sven C. Liebscher, Lars Bannow, Stephan W. Koch

Theoretical Semiconductor Physics Group, Faculty of Physics, Philipps-Universität Marburg

Introduction

In order to predict the optical and electronic properties of novel semiconductor alloys, it is desirable to develop a theoretical approach that does not rely on experimental data, so that promising candidates for technical applications e. g. in solar cells or lasers can be found without the need for extensive experimental testing. Such an approach can be developed using Density Functional Theory, which is an *ab-initio* method capable of finding the groundstate electron density of a given periodic structure. Using the information obtained from DFT, one can calculate microscopic quantities like the polarization by virtue of the Semiconductor Bloch Approach, and thus obtain optical properties like absorption or photoluminescence spectra[1].

Results

In order to simulate GaSb with dilute bismide concentrations within the constraints of periodic boundary conditions found in DFT, GaSb supercells were constructed by placing 4 primitive cells in each direction, yielding supercells with 128 atoms. By replacing single Sb atoms with Bi atoms using a quasi-random distribution that was found by cluster-expansion[2], Bi concentrations of up to 6.25 % were simulated. Since the implementation of Bi atoms changes the forces inside the supercell, the geometry had to be relaxed. To this end, the minimum of the total energy with respect to the supercell volume was found by varying the lattice constant and the ion positions. The results for each Bi concentration are shown in Fig. 1. Afterwards, the bandgap was calculated using the mBJ meta-GGA exchange functional, see Fig. 2. A linear decrease of 29.7 meV/% of the bandgap was found, which is in good agreement with experimental data[3], stating a decrease of 35.6 meV/%.

Outlook

So far, only isotropic supercell geometries have been considered. In order to rule out effects arising from the supercell structure, different geometries should be investigated. Furthermore, in real experiments, the structure can usually relax only in growth direction, resulting in strain effects, which could be simulated by restraining the volume relaxation to one dimension. Additionally, the results of the DFT calculations should be used to study the optical properties of the alloy using the Semiconductor Bloch Approach.

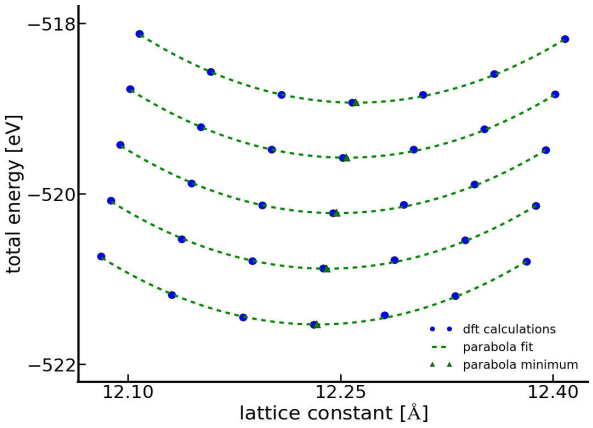

Figure 1: *Variation of total energy with cell volume for different Bi concentrations.*

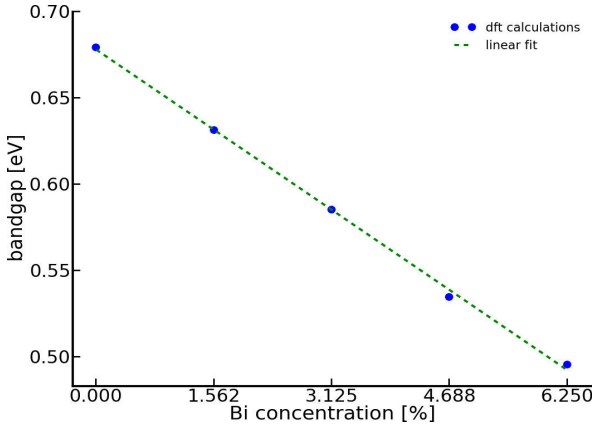

Figure 2: *Bandgap dependence on Bi concentration.*

References

[1] L. C. Bannow, P. Rosenow, P. Springer, E. W. Fischer, J. Hader, J. V. Moloney, R. Tonner, and S. W. Koch, “An ab initio based approach to optical properties of semiconductor heterostructures”, Model. Simul. Mater. Sci. Eng. 25, 065001 (2017).

[2] A. Zunger, S.-H. Wei, L. G. Ferreira, and J. E. Bernard, “Special quasirandom structures”, Phys. Rev. Lett. 65, 353 (1990).

[3] M. P. Polak et al., J. Phys. D: Appl. Phys. 47, 355107 (2014).

IONOTHERMAL APPROACH AND CHARACTERIZATION OF TELLURIDOMERCURATES

B. Peters and S. Dehnen

Philipps-Universität Marburg, Hans-Meerwein-Straße 4, Marburg/D

Because of the semi-conducting properties of chalcogenido metalates, their synthetic access has been subject for several decades.[1,2] Therefore, various studies addressing various synthesis methods were undertaken, which our group extended to an ionothermal approach. This method is based on the usage of so-called ionic liquids (ILs). The broad spectrum of modifications of this reaction method causes the chalcogenido metalate synthesis to be very flexible.[3] Especially the utilization of heavy-element combinations exhibits the possibility of fine-tuning of electronic properties.[4]

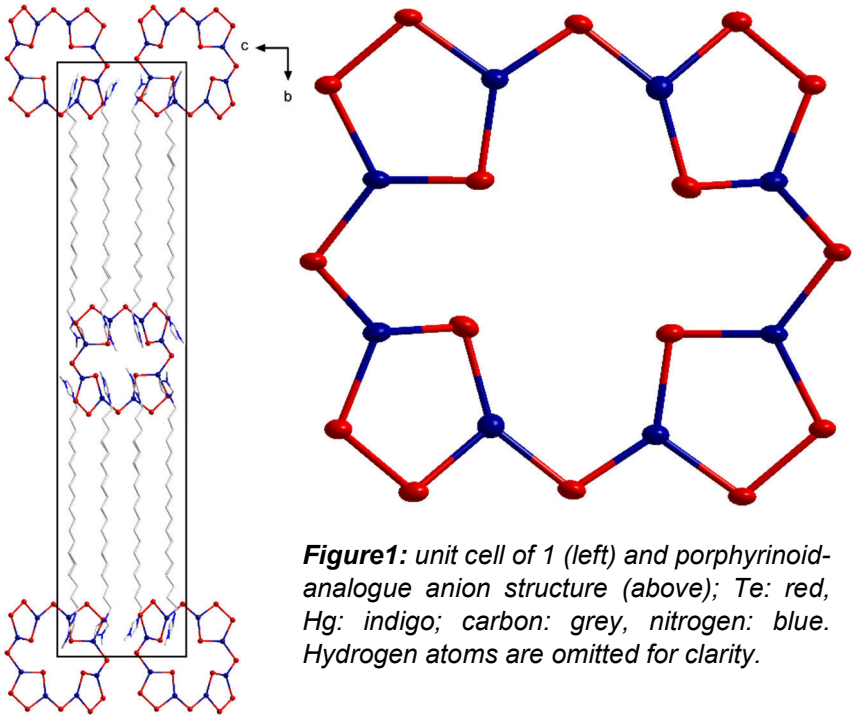

Figure1: *unit cell of 1 (left) and porphyrinoid-analogue anion structure (above); Te: red, Hg: indigo; carbon: grey, nitrogen: blue. Hydrogen atoms are omitted for clarity.*

We successfully obtained four variants of the tellurido metalate $[Cat]_8[Hg_8Te_{16}]$, containing the $[Hg_8Te_{16}]^{8-}$ anion with a porphyrin-related ring structure.[5] Imidazolium cations (Cat) act as counterions. The crystal structure of the compound shows a lamellar assembly of layers comprising anions and imidazolium rings besides layers of the unpolar alkyl chains of the imidazolium derivatives. This circumstance is an excellent precondition for the generation of nanostructured sheets via exfoliation.[6] We aim at a deposition of the exfoliated product onto semiconducting surfaces for investigating their influence on the semiconductor properties.

References

[1] N. Zheng, X. Bu, P. Feng, *Nature* **2003**, *426*, 428–432.
[2] N. Zheng, X. Bu, B. Wang, P. Feng, *Science* **2002**, *298*, 2366–2369.
[3] M. G. Kanatzidis *Inorg. Chem.* **2017**, *56*, 3158–3173.
[4] Y. Pei, C. Chang, Z. Wang, M. Yin, M. Wu, G. Tan, H. Wu, Y. Chen, L. Zheng, S. Gong, T. Zhu, X. Zhao, L. Huang, J. He, M. G. Kanatzidis, L.-D. Zhao *J. Am. Chem. Soc.* **2016**, *138*, 16364−16371.
[5] C. Donsbach, K. Reiter, D. Sundholm, F. Weigend, S. Dehnen, *Angew. Chem. Int. Ed.* **2018**, *57*, 8770–8774.
[6] L. Dou, A. B. Wong, Y. Yu, M. Lai, N. Kornienko, S. W. Eaton, A. Fu, C. G. Bischak, J. Ma, T. Ding, N. S. Ginsberg, L.-W. Wang, A. P. Alivisatos, P. Yang, *Science* **2015**, *349*, 1518–1521.

Opto-Dynamical Properties of Bismuthide III-V Semiconductors

Julian Veletas[1)], Thilo Hepp[2)], Kerstin Volz[2)], and Sangam Chatterjee[1)]

[1)] *Institute of Experimental Physics I and Center for Materials Research, Justus Liebig University Gießen*
[2)] *Faculty of Physics and Material Sciences Center, Philipps-University Marburg*

Dilute bismuth-containing semiconductor alloys such as Ga(As,Bi) are attracting significant attention due to their promising characteristics in near- and mid-infrared laser applications. Beside the use as an active medium for telecommunication wavelength lasers, bismuthide semiconductors offer the possibility of lasers with even longer wavelength and, in general, a wide scope for band structure engineering.[1]

The incorporation of bismuth leads to a strong reduction of the band gap commonly described by an anti-crossing model (VBAC) of the dispersionless Bi-level with the valence bands of the host material.[2] Consequently, the band gap narrows and the separation Δ_{SO} between the valence band edge and the split-off band increases. If Δ_{SO} surpasses E_g, this leads to a suppression of non-radiative Auger recombination and, thus an enhanced performance of future devices. For example, Δ_{SO} surpasses the band gap energy E_g for more than 4 % bismuth incorporation in (Ga,In)(As,Bi) alloys with In concentrations of about 50 %.[3]

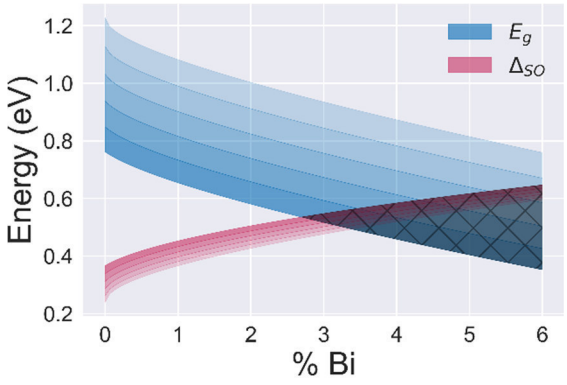

Figure 1 *Critical point energies simulated using the VBAC model as a function of In (darker shading) and Bi fraction.*

In a second project, Ga(As,Bi) based W-structures are realized. Therefore, Ga(As,Bi)/Ga(N,As) and Ga(As,Bi)/(Ga,In)As structures are investigated.

My part of this project addresses the optical properties of these material systems. Therefore, we use several spectroscopy techniques to obtain detailed information about the materials critical points, the emission characteristics, and carrier-relaxation processes. Figure 2 shows modulation and luminescence data of a Ga(As,Bi)/(Ga,In)As structure. Combining the results of these experiments enables an unambiguous identification and analysis of the involved transitions. In future experiments, the dynamics of this charge transfer process will be investigated.

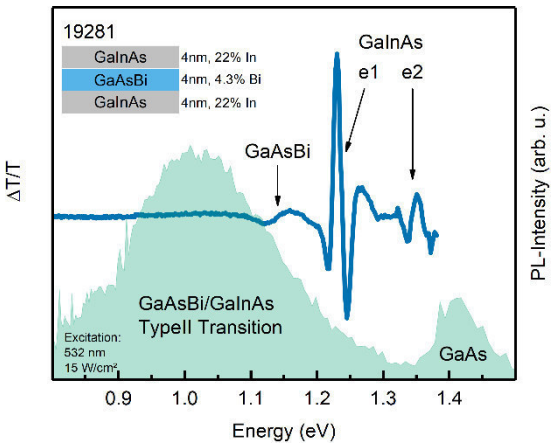

Figure 2 *Modulation Spectroscopy (blue line) and photoluminescence spectra (green shaded) of a Ga(As,Bi)/(Ga,In)As heterostructure reveal the type II transition.*

[1] Jin et al., Appl. Phys. Lett. **114**, 213103 (2013)
[2] Alberi et al., Appl. Phys. Lett. **91**, 051909 (2007)
[3] Marko et al., Appl. Phys. Lett. **101**, 221108 (2012)

In-situ TEM Growth Investigations of III/V Semiconductor Materials

Maximilian Widemann, David Krug, Andreas Beyer, Kerstin Volz

Materials Sciences Center and Faculty of Physics, Philipps University Marburg

Introduction

III/V semiconductors are used for many technical applications, like for example LEDs, lasers and solar cells. A widely used fabrication process of these materials is metal organic vapor phase epitaxy (MOVPE). However, structural investigations of the samples are usually carried out post growth. *In-situ* studies of the growth process promise an improvement of the performance of the fabricated materials. But it comes along with several challenges, like the realization of the growth conditions inside a TEM or the incongruent evaporation of the group V compound at elevated temperatures. *In-situ* (scanning) transmission electron microscopy ((S)TEM) allows to investigate dynamic processes, which occur during the thermal annealing or the growth of III/V semiconductor materials inside a TEM. Gas environmental cell and heating holders enable to supply gases while heating the sample, so that conditions comparable to those during the MOVPE process can be realized in any electron microscope[1].

Methods

To this end, a commercially available Protochips *in-situ* system has been modified. In order to allow the usage of toxic and pyrophoric gases, like the precursor gases used in MOVPE growth a gas mixing system, an appropriate gas monitoring system as well as a gas scrubbing system have been added to the setup[2]. A sample preparation technique is necessary, which allows a controlled transfer of a microscopic and electron transparent sample onto a micro electro mechanical system (MEMS) chip of gas environmental cell holder[3]. This is given by the focused ion beam (FIB) lift out technique and was performed in a JEOL JIB-4601F dual beam system. A double C_S-corrected JEOL JEM 2200FS operating at 200 kV was used for the TEM observations. As a model system GaP nanowires (NW) have been investigated in first growth experiments, since their growth observation comes along with less challenges compared to layer growth processes. Precursor gases used for GaP based experiments are tertiarybutylphosphine (TBP) and trimethylgallium (TMGa). Additionally, N_2 can be used as carrier gas.

Obviously, there is a huge geometrical difference between macroscopic bulk samples and microscopic TEM samples, which have a much higher surface to volume ratio. Nevertheless, thermal stability of these samples under elevated temperatures, which are required for annealing or crystal growth, can be achieved like it is done for bulk samples by a surplus of the group V precursor gas[2]. Furthermore the microscopic geometry of the closed cell holder, which acts as MOVPE reactor, is capable of decomposing the precursor gases and grow crystalline materials from gas phase.

NW vapor liquid solid (VLS) growth experiments catalyzed by gold nanoparticles (NP) have been performed with a total pressure of 400 hPa and precursor partial pressures between 10^{-1} hPa and 10^{-3} hPa with a V/III ratio of 10. Growth temperature has been varied between 400 °C and 450 °C.

Results

The experiments demonstrate the influence of the growth parameters on the NW morphology and growth rate. Temperature strongly determines the shape of the NWs. At 450 °C grown samples show a linear growth behavior, whereas NWs grown at 400 °C form many kinks. Measurements of these kinking angles show a predominance of 70° (Fig. 1a). This is most probably caused by twin boundaries (Fig. 2b)[4]. This defect appears on the gallium terminated (111) surfaces[5]. The reason why the 70° angle is formed more often than the 110° angle, which might be caused by this defect as well, may be given by the conservation of the layer formation order, which is from gallium to phosphorus.

The growth rate of the NWs can be controlled mainly by the partial pressures of the precursor gases. Higher partial pressures lead to an increased incorporation of growth material. Another crucial factor for the growth rate is given by the surface ratio of droplet and growth plane. NWs with different surface ratios can be seen in the STEM images in Fig. 2a during the growth at 450 °C and partial pressures of 1.6×10^{-2} hPa (TBP) and 1.8×10^{-3} hPa (TMGa). The wires show a big difference in the surface ratios, resulting in growth rates of 39.9 nm/s and 2.7 nm/s under the same conditions respectively. Since the incorporated material needs to diffuse through the liquid catalyst, a higher droplet surface leads to higher diffusion. Whereas an increased interface area between droplet and growth plane reduces the growth rate. Fig. 2b shows the growth rate for 13 different NWs of this experiment in dependence of their surface ratios, indicating a linear proportionality.

Furthermore, we compare the growth of nanowires in post growth investigations with applying the same growth conditions with and without electron beam, respectively. All in all, the electron beam seems to have a negligible influence on nanowire growth under appropriate conditions. This suggests that results, collected in *in-situ* TEM growth investigations, can be transferred to processes appearing in conventional MOVPE growth.

Outlook

In further *in-situ* growth experiments, the detailed dependencies of temperature and precursor partial pressures as well as the catalyst droplet geometry on the growth rate needs to be investigated. Also images and videos of atomic resolved layer formation is still missing. To achieve this, a sample preparation technique is needed to prepare NWs on a substrate, which determines the crystal orientation. Since the closed gas cell holder has only single tilt capabilities, it is only reliable to tilt NWs into zone axis with control over the crystal orientation. Additionally, atomic resolved images of twin boundaries causing the 70° kinking angles are to come.

Moreover the insights gained in *in-situ* TEM growth investigations need to be transferred to growth mechanisms like they appear in the MOVPE layer growth. Such experiments require substrate samples in zone axis, which can be achieved by the FIB lift out technique. This promises a deeper understanding of the processes taking place in a MOVPE growth machine, leading to the improvement of grown materials properties.

References

[1] L. F. Allard et al. "A new MEMS-based system for ultra-high-resolution imaging at elevated temperatures." *Microscopy research and technique* 72.3 (2009): 208-215.

[2] R. Straubinger et al. "In Situ Thermal Annealing Transmission Electron Microscopy (TEM) Investigation of III/V Semiconductor Heterostructures Using a Setup for Safe Usage of Toxic and Pyrophoric Gases." *Microscopy and Microanalysis* 23.4 (2017): 751-757.

[3] R. Straubinger, A. Beyer, and K. Volz "Preparation and loading process of single crystalline samples into a gas environmental cell holder for in situ atomic resolution scanning transmission electron microscopic observation." *Microscopy and Microanalysis* 22.3 (2016): 515-519.

[4] M. Zhang et al. "Formation mechanisms for the dominant kinks with different angles in InP nanowires." *Nanoscale research letters* 9.1 (2014): 211.

[5] A. Beyer et al. "Influence of crystal polarity on crystal defects in GaP grown on exact Si (001)." *Journal of Applied Physics* 109.8 (2011): 083529.

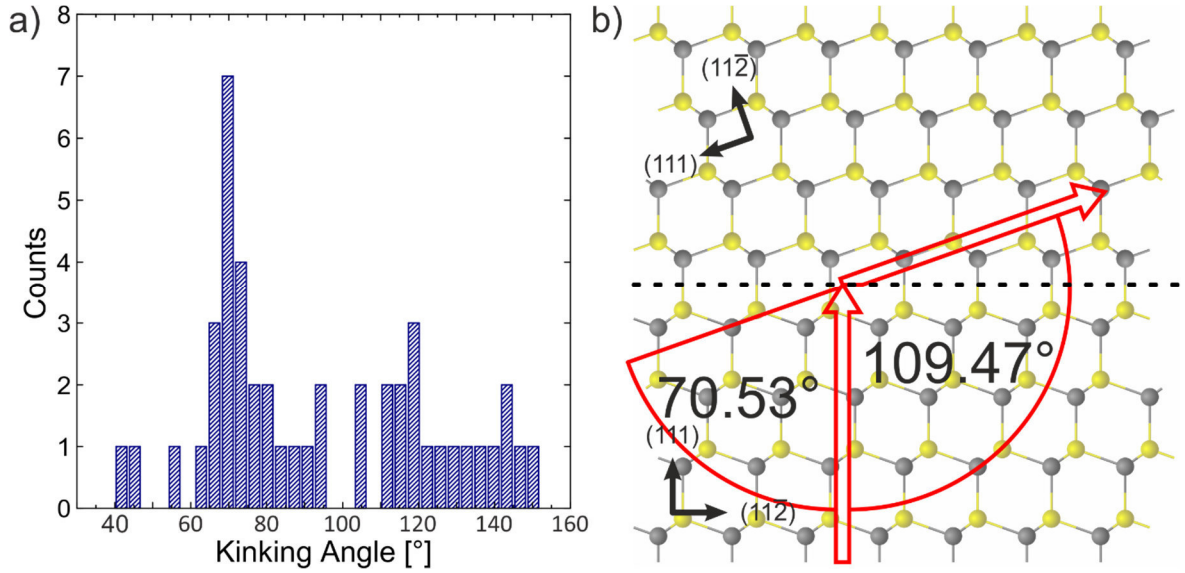

***Figure 1**: a) Histogram of kinking angles of NWs grown at 400 °C. The predominance of 70° indicates twin boundary defects causing these kinks. b) Schematic drawing of a twin boundary (black line) in [1$\bar{1}$ 0] projection.*

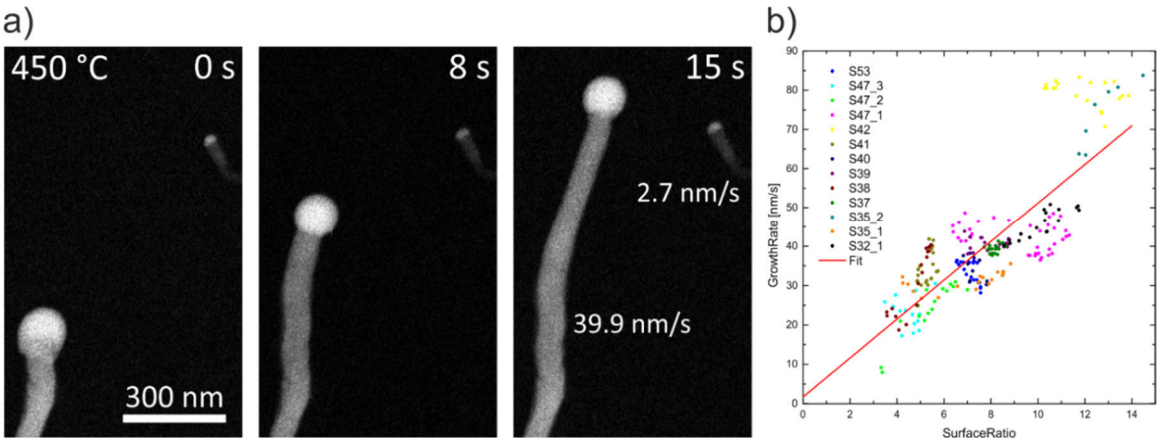

***Figure 2**: a) STEM images of two growing NWs. The deviating surface ratios lead to different growth rates. b) Growth rate measurements of 13 NWs in dependence of their surface ratio. Each color represents a single NW.*

Teilnehmer GRK-Seminar

vom 23.09. - 25.09.2019
Haus Schönblick / Schwäbisch Gmünd

Adamkiewicz	Alexa
Dornsiepen	Eike
Dunaj	Tobias
Glaser	Timo
Glowatzki	Johannes
Günkel	Robin
Heimes	Damien
Hepp	Thilo
Köster	Marcel
Kröner	Marcel
Liebscher	Sven Christian
Maßmeyer	Oliver
Mondal	Badal
Peters	Bertram
Pieck	Fabian
Ritter	Christian
Rost	Luise
Veletas	Julian
Widemann	Maximilian
Wilhelm	Mikko
Youngkin	Steven

Chatterjee	Sangam	Prof. Dr.
Dehnen	Stefanie	Prof. Dr.
von Hänisch	Carsten	Prof. Dr.
Heimbrodt	Wolfram	Prof. Dr.
Mette	Gerson	Dr.
Volz	Kerstin	Prof. Dr.

Hier findet der Workshop statt:

Schönblick
Christliches Gästezentrum Württemberg
Willy-Schenk-Straße 9
73527 Schwäbisch Gmünd
E-Mail: info@schoenblick.de
Telefon: 07171 / 9707-0
Fax: 07171 / 9707-172

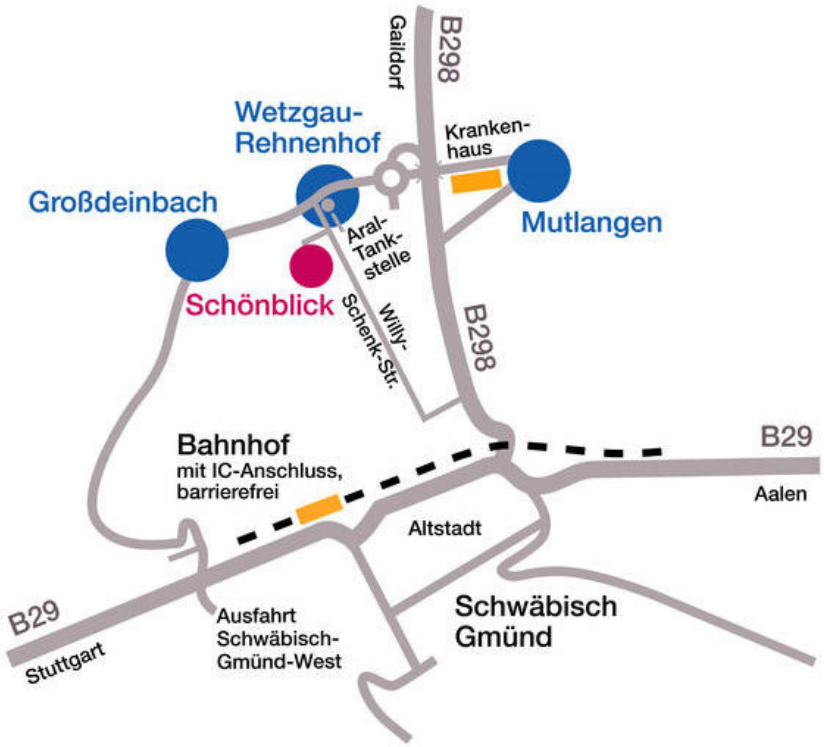

Sie erreichen Haus Schönblick mit dem Auto

Aus Richtung Stuttgart

Fahren Sie auf der B 29 die Ausfahrt Schwäbisch Gmünd-West/Großdeinbach ab. Über Großdeinbach fahren Sie bis Wetzgau. In Wetzgau biegen Sie vor der Aral Tankstelle rechts ab. Der Schönblick ist ausgeschildert. Nach ca. 500 m liegt rechts das Christliche Gästezentrum Württemberg Schönblick.

Von Schwäbisch Gmünd

In Schwäbisch Gmünd fahren Sie Richtung Mutlangen auf der B 298. Sie folgen der Ausschilderung zur Stauferklinik, bis der "Schönblick" ausgeschildert ist.

oder mit öffentlichen Verkehrsmitteln

Ab Hauptbahnhof oder Stadtmitte ist der Schönblick leicht mit der Buslinie 6 - Rehnenhof/Wetzgau zu erreichen. Die Haltestelle Karlsbader Straße liegt direkt vor dem Schönblick.

Aktuelle Busfahrpläne der Gmünder Stadtbusse finden sie unter: https://www.stadtbus-gmuend.de/36.php.